ANALYSIS OF THE TRIBOLOGICAL BEHAVIOR IN TRANSVERSELY ISOTROPIC MATERIALS UTILIZING ANALYTICAL AND FINITE ELEMENT METHODS

by

Xinguo Ning

B.S., Northeastern Institute of Heavy Machinery, 1985

M.S., Huazhong University of Science and Technology, 1988

Submitted to the Graduate Faculty of

School of Engineering in partial fulfillment

of the requirements for the degree of

Doctor of Philosophy

University of Pittsburgh

2002

UNIVERSITY OF PITTSBURGH

SCHOOL OF ENGINEERING

This dissertation was presented

by

Xinguo Ning

It was defended on

December 11, 2002

and approved by

Anne M. Robertson

William S. Slaughter

Patrick Smolinski

James H.-C. Wang

Michael R. Lovell
Dissertation Director

ABSTRACT

ANALYSIS OF THE TRIBOLOGICAL BEHAVIOR IN TRANSVERSELY ISOTROPIC MATERIALS UTILIZING ANALYTICAL AND FINITE ELEMENT METHODS

Xinguo Ning, PhD

University of Pittsburgh, 2002

This dissertation develops methods for evaluating the tribological behavior of anisotropic materials. The underlying objectives of the work are: (1) to elucidate the relationship between the sliding frictional contact and the fiber orientations of FRP composites; (2) to explore the relationship between the anisotropic strength and the wear of FRP composites and develop an innovative wear model of FRP composites; and (3) to derive a general approximate solution for analyzing the contact behavior of transversely isotropic coatings such solid lubricant films.

The first goal was achieved in two steps. First, by incorporating anisotropic contact theory, the elastic properties of FRP composites, and the analytical expressions of Barnett-Lothe tensors, the contact behavior of FRP composites in the three principal fiber orientations (transverse, normal, parallel) was deduced. Specially, the influence of fibers, matrices, volume fractions, and friction coefficients on the contact behavior was ascertained. Next, through the numerical solution of the explicit expressions of Barnett-Lothe tensors, the relationship between the contact performance and the arbitrary fiber orientations was examined. Based on this approach, the influence of fiber orientations on the contact pressure and the contact patch was determined.

To develop an anisotropic wear model of FRP composites, the Tsai-Wu failure strength criterion was employed to establish the relationship between the wear and the contact stress. The theoretically predicated results were in good agreement with the previously published experimental data. This correlation demonstrates that the anisotropic failure strength criteria may be used to explain the anisotropy of wear in FRP composites.

Finally, a set of approximate solutions for thin, transversely isotropic coatings was derived to gain deep insight into the coated structures. These easy-to-use solutions are helpful for optimizing the contact behavior of thin coatings used in the design of contacting components.

DESCRIPTORS

Anisotropic
Coating
Composites
Contact Behavior
Fiber Reinforced Polymer
Friction
Tribology
Wear

ACKNOWLEDGMENTS

I am deeply indebted to my advisor, Dr. Michael Lovell for his guidance, support, collaboration and encouragement throughout my education and research. I also would like to gratefully thank Dr. William Slaughter for his guidance and collaboration on the mechanics analysis of this research. I deeply appreciate Dr. James Wang, who not only serves on my committee but also is generous to give me great help. I am equally indebted to my advisory committee members, Dr. Patrick Smolinski, and Dr. Anne Robertson, for their providing invaluable suggestions towards this research.

I gratefully thank Mr. Clint Morrow for his collaboration and discussion about the content in chapter 5. I am grateful for the support of the Department of Mechanical Engineering at University of Pittsburgh. My thanks also go to ANSYS Inc. for their offering me the 2001 summer internship. I also thank Mr. Grama Bhashyam, Dr. Guoyu Lin and Dr. Jin Wang at ANSYS Inc. for their guidance.

Finally, I wish to express my deep appreciation to my dear parents and brother and sisters for their support, affection and inspiration throughout my education.

TABLE OF CONTENTS

LIST OF TABLES

LIST OF FIGURES

NOMENCLATURE

a	left width of the contact patch
A	transformation matrix
b	right width of the contact patch
c	elastic constant
C	compliance matrix
$\hat{e}$	orthonormal vector basis
E	Young's modulus
f	friction coefficient or subscript represents fiber
F	applied normal force
G	shear modulus
H	material hardness
i	subscript, i=1…6
j	subscript, j=1…6
k	wear factor
K	bulk modulus
L	Barnett-Lothe tensor
m	subscripts expressing the resin
p(x)	pressure distribution

r	radius of curvature of the parabolic cylinder
R	matrix
S	Barnett-Lothe tensor
S_s	shear strength
t	layer thickness and subscript represents transverse or tensile
T	matrix
u	displacement
v	sliding direction
V	volume fractions
$\dot{w}$	wear rate
X_c	compressive strength in X-axis
X_t	tensile strength in X-axis
y(x)	indenter profile
Y	yield stress
Y_c	compressive strength in Y-axis
Y_t	tensile strength in Y-axis
α	parameter
β	characteristic parameter
ν	Poisson's ratios
σ_i	normal stress components
ε_i	normal strain components
τ_{ij}	shear stress components
η	parameter

δ characteristic parameter

γ_{ij} shear strain components

ξ sin(θ)

ζ cos(θ)

ρ parameter

λ parameter

1.0 INTRODUCTION

The word *tribology*, derived from the Greek word *tribos* meaning rubbing, first appeared in Jost's report [1] and was defined as: '… The science and technology of interacting surfaces in relative motion and the practices related thereto.' As interdisciplinary science and technology, it includes friction, wear and lubrication.

Tribology is crucial to modern industry. Many tribological components such as brakes, clutches, driving wheels, bolts, nuts, gears, cams, bearings, and seals are applied in the machinery. The friction and wear appearing in these operations is one of the largest energy losses. It was estimated in 1966 [1] that the United Kingdom could save approximately 500 million pounds per year, and the United States could save in excess of 16 billion dollars per year by better tribological designs. Therefore, research in tribology may lead to substantially economical saving and better performance of machines.

The commonly used materials in tribological components range from metals, alloys to ceramics, solid lubricants, polymers, and composites. Among these materials, several are transversely isotropic in nature such as unidirectional continuous fiber-reinforced polymer (FRP) composites, and molybdenum disulphide (MoS_2). The former material is a class of tribological materials that possess unique self-lubricating capability and low noise, and the latter one represents an important solid lubricant that may be coated on the surfaces of tribological components to meet the severe work conditions and often reduce the cost. FRP composites and coated structures are widely utilized in tribological components such as gears, seals, and bearings, and hence have been theoretically and experimentally studied.

1.1 FRP Composites

FRP composite materials are comprised of matrix and fiber elements. The fibers of FRP composites give them their unique mechanical characteristics. The most common filled fiber reinforcements are glass, carbon (graphite), and aramid (Kevlar 49). E-glass fibers are created using a calcium aluminoborosilicate formulation that produces beneficial mechanical properties at very reasonable cost. Carbon or graphite fibers are currently the best known and most widely utilized high performance composite. Aramid is a class of aromatic–polyamide fibers that are produced using para-phenylene terephthalamide. The purpose of the FRP composite matrix material is to bind the fibers together. By virtue of their cohesive and adhesive characteristics, the resins give FRP materials the ability to transfer load to and between fibers, and to protect them from environmental conditions and handling. The most common matrix materials are epoxy, PEEK (polyether ether keton), and PPS (polyphenylene sulfide).

With numerous possible material combinations, FRP composites provide nearly unlimited possibilities for optimizing the tribological performance of mating components. For this reason, polymer composites are widely utilized in numerous applications including seals, bearings, gears, and artificial prosthetic joints.

1.1.1 Wear Anisotropy Of FRP Composites

Unidirectional continuous fiber-reinforced polymer composites exhibit significant tribological anisotropy due to their heterogeneity. As described in the literature [2-6], fiber orientations have a significant influence on the wear and friction behavior of FRP composites.

Experimental investigation has shown that the largest wear resistance in FRP composites occurred when the sliding was normal to the fiber orientation, while the lowest wear resistance occurred when the fiber orientation was in the transverse direction. Experiments have also shown that the coefficient of friction and the wear in FRP composites depend on several factors including the material combination, the fiber orientation, and the surface roughness. Sung and Suh [2] tested T300/epoxy and Kevlar 49/epoxy composites and explained the wear phenomena using a delamination theory. In their work, the wear was found to be related to the stress field under the indentation of an asperity, the mechanics of the crack nucleation and propagation, and the material properties.

Tsukizoe and Ohmae [7] later performed numerous experiments to establish the influence of fiber orientation, elastic modulus, loading condition, friction coefficient, interlaminar shear strength, and the fracture strain on the wear rate of FRP composites. Based on the experimental results, they proposed the following empirical wear rate equation:

$$\dot{w} = \rho\left(\frac{fp}{E}\right)^{\lambda}\frac{1}{I_s} \tag{1.1}$$

where ρ is the wear constant; λ is an exponential parameter; f is the friction coefficient; p is the applied pressure; E is the elastic modulus and I_s is the interlaminar shear strength. By means of the above empirical wear equation, Lhymn [3] investigated the tribological properties of unidirectional polyphenylene sulfide-carbon fiber laminate composites. He attempted to qualitatively explain the effect of fiber orientation in terms of the difference in the interlaminar shear strength and the fracture strain of the three principal fiber orientations. In order to theoretically elucidate the effect of fiber orientation on the wear of composites, Ovaert and Wu

[8, 9] constructed a relationship between the wear rate of normally oriented FRP composites and the fiber debonding depth under the indentation of a spherical asperity. For the wear of FRP composites in the parallel-oriented fiber orientation, Ovaert [10, 11] later introduced a model of a beam lying on a foundation to simulate the fibers in a polymer matrix. These models clearly demonstrate the wear modes in the three principal directions and the influence of the microstructures of FRP composites on the wear.

1.1.2 Contact Pressure Of FRP Composites

The classical Hertzian contact theory cannot be applied to anisotropic materials such as FRP composites, so several researchers have analyzed the contact between anisotropic bodies. Klingworth and Stronge [12] analyzed a plane punch indentation of anisotropic elastic half space with the potential function approach. Fan and Keer [13] derived a general solution for two-dimensional contact on anisotropic half-space by combining the approach of analytical continuation [14] and Stroh's formalism [15]. This method can be used to evaluate the in-plane deformation and the coupled deformation between the in-plane and the anti-plane. Fan and Hwu [16-18] studied general contact problems for an anisotropic elastic half-plane and obtained the closed-form solutions for the sliding contact of bodies on anisotropic elastic planes. Recently, Ning and Lovell [19, 20] revealed the contact behavior for arbitrary fiber orientations of unidirectional continuous FRP composites and highlighted the correlation between the contact characteristics and the wear.

1.2 Contact Problems Of Coating Structures

Surface coatings have become widely utilized in the engineering community due to the many potential benefits they offer. These coatings, which may be isotropic or anisotropic in nature, are typically used to enhance the contact characteristics and improve the tribological performance of mating components. One of the most common applications for surface coatings is in rolling element or slider bearings that operate in vacuum or low temperature environments. As described in the literature [cf. 21], oils and other liquid lubricants may evaporate in vacuum and contaminate instrumentation. At low temperature, fluid lubricant viscosity dramatically increases and may become insufficient over time. In such applications, solids lubricant coatings are often the most effective method of reducing wear in contacting components. Coatings are generally very thin layers of soft metals (e.g. Au, Ag, In, and Pb), laminar solids (e.g., MoS_2 and Boron Nitride), or polymers (e.g., PTFE, Polyamide composites and Phenolic and Epoxy), which are deposited onto a substrate surface.

When solid lubricant coatings are applied to a substrate, the contact stress and displacement fields significantly deviate from the Hertzian contact profile within the half-space. This causes significant problems to designers because there are no closed-form solutions available for analyzing three-dimensional coated surface contact for even simple geometries. Reviewing the literature, various researchers have analytically investigated axi-symmetrical contact problems with isotropic elastic layers. Sneddon [22] expressed the axi-symmetrical punch stress and displacement in the layer in terms of Hankel integral transforms. Chen [23], and Chen and Engel [24] studied multi-layered media by respectively employing the Fourier integral transform and the least square integral approach. Matthewson [25] approximated the stress

within thin compliant layers by averaging through the layer thickness. Aleksandrov [26] obtained asymptotic solutions for the stresses in a layer and Jaffar [27] gave a numerical solution for the contact traction and displacement by using modified Legendre polynomials. O'Sullivan and King [28] analyzed sliding contact of a sphere on an elastic layered half-space and determined the stress fields using the Papkovich-Neuber potentials. Johnson [29] developed an approximate method based on the assumption that " plane sections remain plane after compression", and analyzed frictionless cylinder indenting an unbonded or bonded layer on a rigid foundation. His solution was found to be in good agreement with Meijers' [30] when the ratio of contact semi-width to layer thickness is large. Jaffer [31] later employed Johnson's assumption to obtain an asymptotic solution for the axi-symmetrical indentation of a thin elastic layer bonded or unbonded to a rigid foundation. Barber [32] extended the same assumption to general three-dimensional isotropic elastic thin layer punch problems with arbitrary shaped indenters. Tian and Bhushan [33] analyzed the contact of 3-dimensional layered with rough surfaces by variational principle.

Anisotropic coatings demonstrate more complicated contact characteristics than isotropic elastic layers because of their directional dependence. Ovaert [34] analyzed the punch problem of a rigid ellipsoidal indenter on a transversely isotropic solid lubrication film. Kuo and Keer [35] obtained numerical solutions for transversely isotropic multi-layered media by means of Hankel transforms. Lovell et al. [21, 36, 37] used finite element method to investigate the normal stress and tangential friction characteristics of an elastic sphere in contact with transversely isotropic, coated elastic substrate surface.

1.3 Motivations

For the purpose of fully utilizing the beneficial tribological characteristics of FRP composites, it is necessary to obtain an in-depth knowledge of their contact behavior and establish the relationship between the wear and the fiber orientations. However, Hertzian and other fundamental contact theories are not valid for FRP composites due to their anisotropy. The present investigation will incorporate the analytical and the explicit expressions of Barnett-Lothe tensors [38, 39] to the analytical solutions to reveal the effect of fiber orientations on the contact behavior and to develop an anisotropic wear model of unidirectional continuous FRP composites.

As reviewed earlier in the chapter, there has not existed an exact closed-form solution for the analysis of the transversely isotropic, layered system. However, a set of approximate analytical solutions may provide not only a convenient design tool to predicate the performance of coating systems but in-depth understanding of the roles of the material properties as well. In this work, approximate solutions will be derived based on specified assumptions.

1.4 Objectives

The present research has two main goals; one is to attempt to elucidate how the fiber orientation affects the wear of unidirectional continuous FRP composites and to model the anisotropic wear, the other is to derive approximate formulae for a thin, transversely isotropic coatings bonded or unbonded on a rigid foundation. To achieve the first goal, there are two steps:

- Propose an analytical approach to investigate the two-dimensional contact behavior of FRP composites, including the effect of fiber orientations, fiber and matrix materials, friction coefficients, and material volume fractions
- Based on anisotropic strength criteria, develop anisotropic wear model for FRP composites

To achieve the second goal, the Johnson's assumption [29] was incorporated in the basic elastic theory.

2.0 ANALYSIS OF TWO-DIMENSIONAL ANISOTROPIC CONTACT

2.1 Problem Formulation

In the present investigation, the unidirectional continuous FRP composites will be modeled as a quasi-homogeneous, transversely isotropic elastic half-space that is in contact with an infinitely long, rigid parabolic cylinder. A Cartesian coordinate system will be defined such that the *Y*-axis coincides with the vertical axis of the cylinder, as shown in Fig. 1. The sliding direction, v, is perpendicular to the axis of cylinder, and motion occurs from left to right. $(-a, b)$ is the interval of the contact patch,

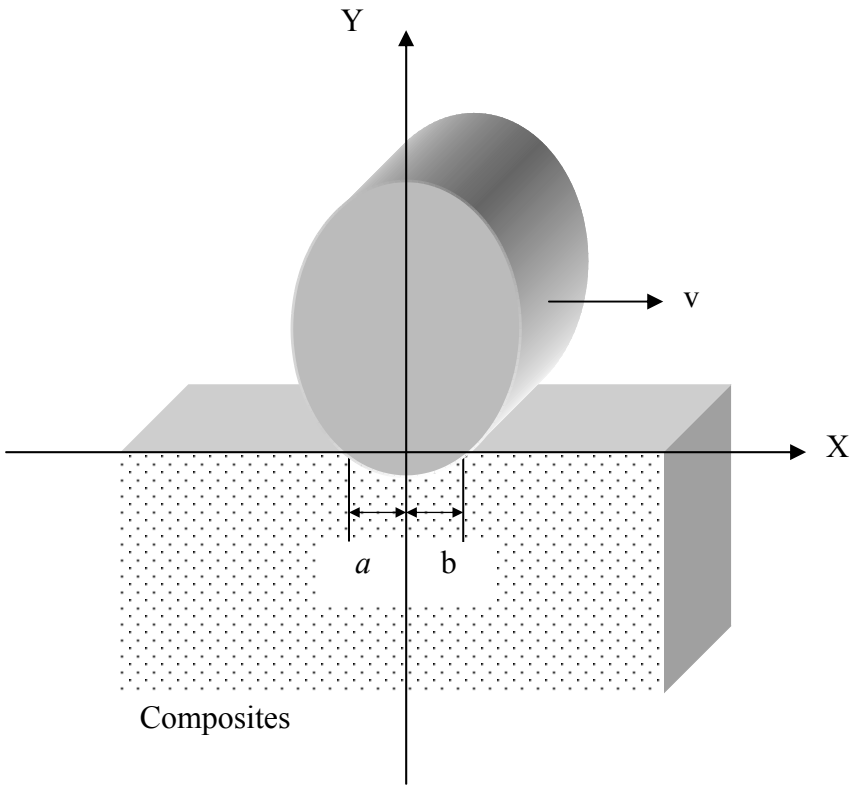

Figure 1 Contact model of a rigid cylinder on FRP composites

2.1.1 Elastic Properties Of Composites

When the coordinates coincide with the principal axes of the elastic half-plane (as in Fig.1), the stress/strain relationship of uni-directional composites can be sufficiently described using five elastic constants. In such a condition the X-Y plane is considered transversely isotropic, and the generalized Hooke's law becomes:

$$\begin{Bmatrix} \sigma_1 \\ \sigma_2 \\ \sigma_3 \\ \tau_{23} \\ \tau_{31} \\ \tau_{12} \end{Bmatrix} = \begin{bmatrix} c_{11} & c_{12} & c_{13} & 0 & 0 & 0 \\ c_{12} & c_{11} & c_{13} & 0 & 0 & 0 \\ c_{13} & c_{13} & c_{33} & 0 & 0 & 0 \\ 0 & 0 & 0 & c_{44} & 0 & 0 \\ 0 & 0 & 0 & 0 & c_{44} & 0 \\ 0 & 0 & 0 & 0 & 0 & c_{66} \end{bmatrix} \begin{Bmatrix} \varepsilon_1 \\ \varepsilon_2 \\ \varepsilon_3 \\ \gamma_{23} \\ \gamma_{31} \\ \gamma_{12} \end{Bmatrix} \tag{2.1}$$

where c_{ij} are the components of material stiffness matrix C, and $c_{66}=(c_{11}-c_{12})/2$; σ_i and ε_i are the normal stress and strain components; and τ_{ij} and γ_{ij} are the shear stress and strain components, respectively. The components of the stiffness matrix may be expressed in terms of engineering constants:

$$c_{11} = c_{22} = \frac{1-\nu_{23}\nu_{32}}{E_2 E_3 \Delta} \tag{2.2}$$

$$c_{12} = \frac{\nu_{21}+\nu_{31}\nu_{23}}{E_2 E_3 \Delta} = \frac{\nu_{23}+\nu_{32}\nu_{13}}{E_1 E_3 \Delta} \tag{2.3}$$

$$c_{13} = c_{23} = \frac{\nu_{31}+\nu_{21}\nu_{32}}{E_2 E_3 \Delta} = \frac{\nu_{13}+\nu_{12}\nu_{23}}{E_1 E_3 \Delta} \tag{2.4}$$

$$c_{33} = \frac{1-\nu_{12}\nu_{21}}{E_1 E_3 \Delta} \tag{2.5}$$

$$c_{44} = c_{55} = G_{23} = G_{31} \tag{2.6}$$

$$c_{66} = G_{12} \tag{2.7}$$

where $\Delta = (1-\nu_{12}\nu_{21}-\nu_{23}\nu_{32}-\nu_{13}\nu_{31}-2\nu_{21}\nu_{32}\nu_{13})/E_1E_2E_3$; E_1 (=E_2) is the elastic modulus in the plane of transverse isotropy; E_3 is the longitudinal elastic modulus normal to the plane of isotropy; ν_{31} is the longitudinal Poisson's ratio and ν_{12} is the transverse Poisson's ratio; and G_{31} and G_{12} are the transverse and the longitudinal shear moduli, respectively.

Unlike those of metals, the elastic constants of FRP composites exhibit the mixed properties of the constituents. If the fiber is assumed to be isotropic, the elastic constants can be determined using the representative elastic properties of the fiber and the matrix, as presented by Rosen [40] and Hashin [41]:

$$E_3 = E_m V_m + E_f V_f + \frac{4V_m V_f (\nu_f - \nu_m)^2}{V_m/k_f + V_f/k_m + 1/G_m} \tag{2.8}$$

$$\nu_{31} = V_m \nu_m + V_f \nu_f + \frac{V_m V_f (\nu_f - \nu_m)(1/k_m - 1/k_f)}{V_m/k_f + V_f/k_m + 1/G_m} \tag{2.9}$$

$$G_{12} = G_m \frac{(\alpha + \beta_m V_f)(1+\rho V_f^3) - 3V_f V_m^2 \beta_m^2}{(\alpha - V_f)(1+\rho V_f^3) - 3V_f V_m^2 \beta_m^2} \tag{2.10}$$

$$E_1 = E_2 = \frac{4k_t G_{12}}{k_t + G_{12}(1 + 4k_t \nu_{31}^2 / E_3)} \tag{2.11}$$

$$\nu_{12} = E_1 / 2G_{12} - 1 \tag{2.12}$$

$$\frac{E_i}{\nu_{ij}} = \frac{E_j}{\nu_{ji}} \ , \quad (\ \mathrm{i, j} = 1, 2, 3\ ) \tag{2.13}$$

$$G_{31} = G_m \frac{V_m G_m + (1+V_f) G_f}{V_m G_f + (1+V_f) G_m} \tag{2.14}$$

$$k_t = \frac{k_m k_f + (V_f k_f + V_m k_m) G_m}{V_m k_f + V_f k_m + G_m} \tag{2.15}$$

$$\alpha = (\gamma + \beta_m)/(\gamma - 1) \tag{2.16}$$

$$k_f = E_f / 2(1 - \nu_f - 2\nu_f^2), \quad k_m = E_m / 2(1 - \nu_m - 2\nu_m^2) \tag{2.17}$$

$$\beta_m = 1/(3 - 4\nu_m), \quad \beta_f = 1/(3 - 4\nu_f), \tag{2.18}$$

$$\rho = (\beta_m - \gamma\beta_f)/(1 + \gamma\beta_f), \quad \gamma = G_f / G_m \tag{2.19}$$

where k is the bulk modulus; V is the volume fraction of the fiber or the matrix; and the subscripts f, m, and t respectively express the fiber, matrix, and transverse.

2.1.2 Boundary And Frictional Conditions

In the case of two-dimensional sliding contact, the boundary conditions on the anisotropic half-plane are given by:

$$\tau_{12} = f\sigma_{22}, \quad -a \le x \le b \tag{2.20}$$

$$\tau_{12} = \sigma_{22} = 0, \quad x < -a \quad \text{or} \quad x > b \tag{2.21}$$

$$y(x) = \frac{x^2}{2r} \ , \quad -a \le x \le b \tag{2.22}$$

where τ_{12} is the shear stress component on the contact plane in the sliding direction, σ_{22} is the normal stress component on the contact plane, *y(x)* is the mathematical expression of the profile of the indenter, and *r* is the radius of the curvature of the parabolic cylinder,. In Eqs. 2.20-2.22, (-a ,b) is the interval of the contact patch, and f is the friction coefficient of the composite in the direction of the *X*-axis.

Since the problem analyzed in this work assumes steady sliding motion, a dynamic coefficient of friction will be used for f. The composites' frictional coefficients may be calculated using the law of mixtures [7] if the dependence of the frictional coefficient on the reinforcement orientation is negligible:

$$f = (V_f / f_f + V_m / f_m)^{-1} \tag{2.23}$$

In this work, it is assumed that the dependence of the frictional coefficient on the reinforcement orientation might be negligible. It is noted that the friction coefficient varies with the fiber orientation as shown in the previous experimental results [2]. In order to obtain a theoretical solution for the effect of material anisotropy, however, the friction coefficient of composites was assumed to be constant. This is of course a simplification to a more complex phenomenon, but is required for the purpose of obtaining useful analytical results.

2.1.3 Frictional Sliding Contact Pressure

The two-dimensional sliding contact pressure on the anisotropic elastic half-plane may be derived using analytical continuation method [14] and Stroh's formalism [15]. In this case, the following closed-form solutions have been obtained by Hwu and Fan [17]:

$$p(x) = \frac{2\sin(\delta\pi)}{(\beta+\overline{\beta})r}(b-x)^{\delta}(x+a)^{1-\delta} \tag{2.24}$$

$$\delta = \frac{1}{2\pi}\arg(-\frac{\overline{\beta}}{\beta}) \ , \ 0 \le \delta \le 1 \tag{2.25}$$

$$a^2 = \frac{\delta(\beta+\overline{\beta})rF}{\pi(1-\delta)} \tag{2.26}$$

$$b^2 = \frac{(1-\delta)(\beta+\overline{\beta})rF}{\delta\pi} \tag{2.27}$$

where F is the normal applied load, β is a parameter that reflects the anisotropic elastic properties of materials, $\overline{\beta}$ is the conjugate of β, and δ is a parameter to characterize the symmetry of the contact patch with respect to the Y-axis.

Equations 2.24-2.27 describe a two-dimensional contact of a parabolic cylinder on general anisotropic elastic half-plane. The contact pressure distribution is characterized by the parameters of β and δ. The value of β is determined by Barnett-Lothe tensors.

$$\beta = M_{22}^{*} + fM_{21}^{*} \tag{2.28}$$

where M_{ij}^{*} is the components of the Hermitian matrix, given by:

$$M^{*} = (I - iS)L^{-1} \tag{2.29}$$

where I is a unit matrix. L and S are two of three Barnett-Lothe tensors. So the analysis of contact performance involves the determination of the Barnett-Lothe tensors. They appear in the Stroh's formalism of two- or three- dimensional deformations of anisotropic elastic materials. Physically, L (except L_{33}) represents a uniform stress state in an anisotropic elastic solid, and S is related to the strain components [42]. Mathematically, they have different definitions shown in their explicit expressions for generally anisotropic materials.

The values or the expressions of the Barnett-Lothe tensors depend upon the anisotropy of materials. Firstly, the orthotropic materials are discussed. And then generally anisotropic materials are evaluated for the arbitrary fiber orientations.

3.0 CONTACT PERFORMANCE IN PRINCIPAL FIBER ORIENTATIONS

3.1 Elastic Constants Of Orthotropic Materials

If the cylinder slides along the principal fiber orientations, the coordinate axes coincide with the principal axes of the elastic half-space (as in Fig.1). In this case, the material is orthotropic, and the stress and strain of the in-plane and the anti-plane can be decoupled. For example, for the TL orientation, the generalized Hooke's law is simplified as:

$$\begin{bmatrix} \sigma_1 \\ \sigma_2 \\ \tau_{12} \end{bmatrix} = \begin{bmatrix} c_{11} & c_{12} & 0 \\ c_{12} & c_{11} & 0 \\ 0 & 0 & c_{66} \end{bmatrix} \begin{Bmatrix} \varepsilon_1 \\ \varepsilon_2 \\ \gamma_{12} \end{Bmatrix} \tag{3.1}$$

The stress/strain relations corresponding to the sliding contact directions of NL, and PL can be similarly given. As shown in Fig. 2, three different fiber orientations will be considered: (1) the transverse fiber orientation (TL), (2) the normal orientation (NL), and (3) the parallel fiber orientation (PL).

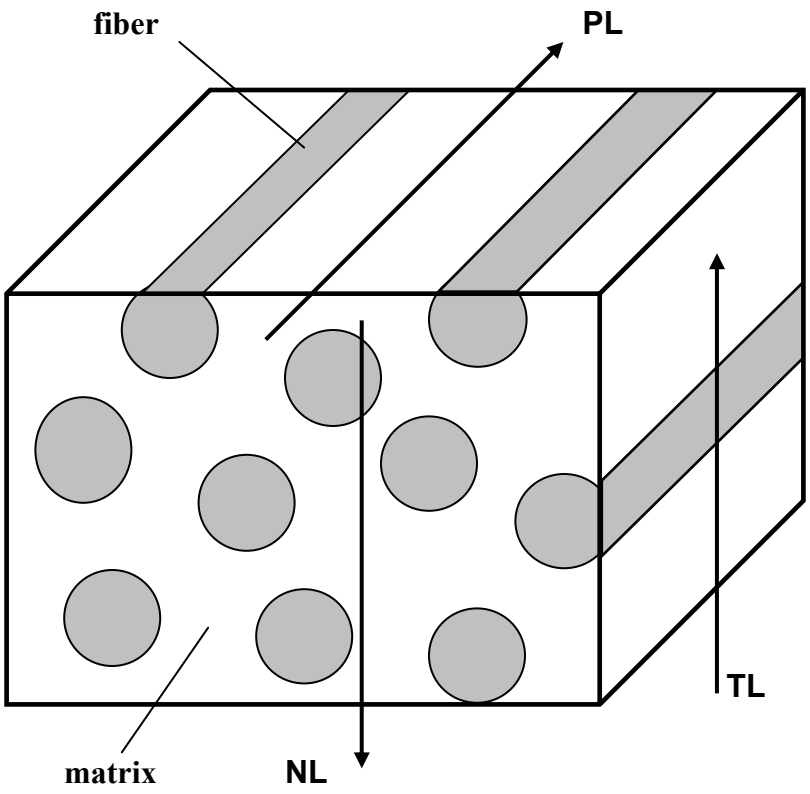

Figure 2 Principal fiber orientations and the sliding direction

3.2 Components Of Barnett-Lothe Tensors

For the contact of two orthotropic elastic bodies, the explicit expression of β is [17]:

$$\beta = \frac{1}{L_{22}^{(1)} L_{22}^{(2)}} \{ L_{22}^{(1)} + L_{22}^{(2)} + if(S_{12}^{(1)} L_{22}^{(2)} - S_{12}^{(2)} L_{22}^{(1)}) \} \tag{3.2}$$

where L_{ij} and S_{ij} are the components of Barnett-Lothe tensors, L and S. Superscripts represent the elastic bodies.

If a rigid body slides on orthotropic materials, the value of $L_{22}^{(1)}$ is infinite, so the value of β reduces to [17]:

$$\beta = \frac{1}{L_{22}} - if\frac{S_{12}}{L_{22}} \tag{3.3}$$

L and S are two of three Barnett-Lothe tensors. The analytical expressions of L and S for orthotropic materials have been given in terms of elastic constants c_{ij} by Dongye and Ting [38]. The non-zero components of the Barnett-Lothe tensors for orthotropic materials are as follows [17]:

$$S_{21} = \left(\frac{c_{66}(\sqrt{c_{11}c_{22}} - c_{12})}{c_{22}(c_{12} + 2c_{66} + \sqrt{c_{11}c_{22}})} \right)^{1/2} \tag{3.4}$$

$$S_{12} = -\sqrt{c_{22}/c_{11}} S_{21} \tag{3.5}$$

$$L_{11} = (c_{12} + \sqrt{c_{11}c_{22}}) S_{21} \tag{3.6}$$

$$L_{22} = \sqrt{c_{22}/c_{11}}L_{11} \tag{3.7}$$

$$L_{33} = (c_{44}c_{55})^{1/2} \tag{3.8}$$

It is important to note that the parameters of β and δ reflect the degree of anisotropy properties and the amount of friction. For smooth surface, the value of δ is 0.5 and the contact profile is symmetrical about the vertical axis of the parabolic cylinder. For surfaces with friction, the contact patch becomes asymmetrical. The value of δ describes the deviation of the maximum contact pressure from the axis of the parabolic cylinder. If the value of δ is less than 0.5, the maximum normal pressure deviates to the side of the moving direction. If δ is larger than 0.5, the maximum normal pressure would deviate in the opposite direction. Usually, the value of δ is less than 0.5, and hence the absolute value of b is larger than that of a in the contact patch.

3.3 Numerical Results And Discussion

Based on the representation of the elastic properties of FRP composites (Eq. 3.1), the mixture law of friction (Eq. 2.23), and the analytical solutions (Eqs. 2.24-2.27), the influence of the material combinations, the fiber orientations and the frictional coefficients on the pressure distributions of FRP composites in three principal alignments can be assessed. In this work, a normal force of 30 N and an indenter radius of 8 mm will be evaluated.

The pressure distributions for a wide range of contact conditions are investigated and plotted in figures. In the figures, the horizontal coordinate is marked according to the fraction of the average contact half-width, x_0.

$$x_0 = (a_1 + b_1)/2 \tag{3.9}$$

In Eq. 3.9, $(-a_1, b_1)$ represents the minimum interval of the contact patch. The vertical coordinate of figures shows the pressure values. From the figures, the variation of the pressure distribution and the contact area can be determined as a function of the fiber materials, the volume fractions, the fiber orientations, the resin materials and the friction coefficient.

3.3.1 Influence Of Fiber Orientations

The influence of the fiber orientation on the two-dimensional contact pressure distribution is illustrated in Fig. 3 for one of the most common FRP composites, epoxy/T300 (see

Table 1). Examining Fig. 3, it is found that the pressure distribution and the contact patch can distinctly vary with the principal fiber orientation. In the figure, the smallest maximum pressure and the largest half-width are obtained when the sliding contact occurs in the transverse (TL) fiber alignment, while the largest maximum pressure and the smallest half-width occur in the normal (NL) fiber orientation. The maximum pressure in the NL orientation is actually more than 300% greater than that of the TL orientation. This can best be explained by investigating the stiffness variability of FRP composites in different orientations. While in the NL fiber orientation, the fibers will carry a significant portion of the normal force as the fibers are axially compressed by the rigid cylinder. This is in contrast to the TL and PL orientations where the fibers experience a predominantly shearing action and the matrix carries the largest portion of the normal load. Examining the material properties of epoxy/T300 FRP given in Table 1, it is found that the fiber is more than 600 times stiffer than the matrix material. Hence, the NL orientation will be far less compliant than the PL and TL orientations, as illustrated in Fig. 3.

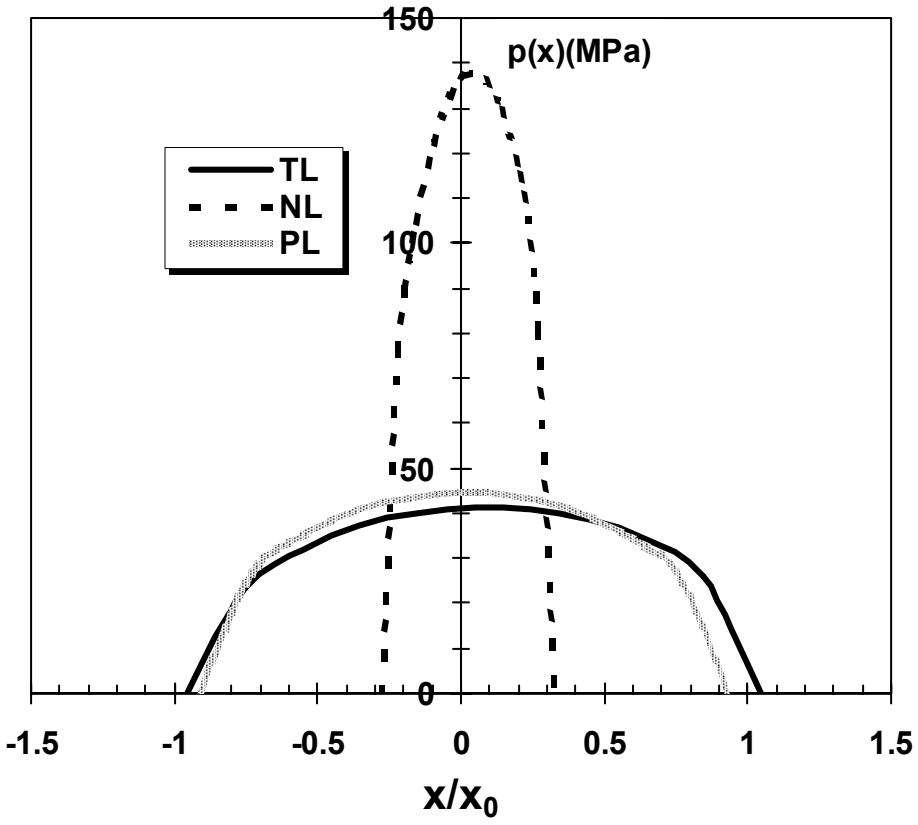

Figure 3 Pressure for Epoxy/T300 in three principal fiber direcitons

In Figure 3 it is also found that the maximum pressure in the PL orientation is slightly larger than that of TL orientation, and that the contact patch in the PL direction is slightly narrower than the TL direction. This difference between the PL and TL directions can be attributed to the contribution of the elastic constant C_{11}. The maximum contact pressure is known to increase with C_{11}. Since C_{11} in the PL orientation is 30 times larger than that of the TL orientation, it is natural for the PL orientation to have a greater pressure distribution and a smaller contact area. It is somewhat surprising, however, that the maximum contact pressure in Fig. 3 does not vary to a greater extent between PL and TL. Such a finding can be attributed to the complex compliance behavior of anisotropic materials.

Table 1 Material properties of Epoxy/T300 FRP composite

FRP	**Fiber**		**Matrix**		**Composites**
Epoxy + T300 (Carbon fiber) [2]	Modulus (GPa)	Poisson's Ratio	Modulus (GPa)	Poisson's Ratio	Frictional Coefficient
	228	0.2	0.33	0.34	0.2

Another important set of information provided by Fig. 3 is the influence of fiber orientation on the symmetry of the contact patch. As shown in the figure and as calculated by Eq. 2.25, the value of δ in the normal fiber orientation is 0.4663. This is the smallest among three

principal fiber orientations, which indicates the maximum contact pressure in the NL alignment deviates the farthest distance from the vertical axis of the cylinder. The value of δ in the parallel (PL) fiber alignment is the highest at 0.4964, which shows that the maximum contact pressure is the nearest to the vertical axis of the cylinder. Such a finding can again be explained by the fact that the NL orientation is very stiff, and therefore has a small contact area than the other orientations. This smaller contact area is more sensitive to deviations caused by friction and anisotropy, thus leading to small δ values.

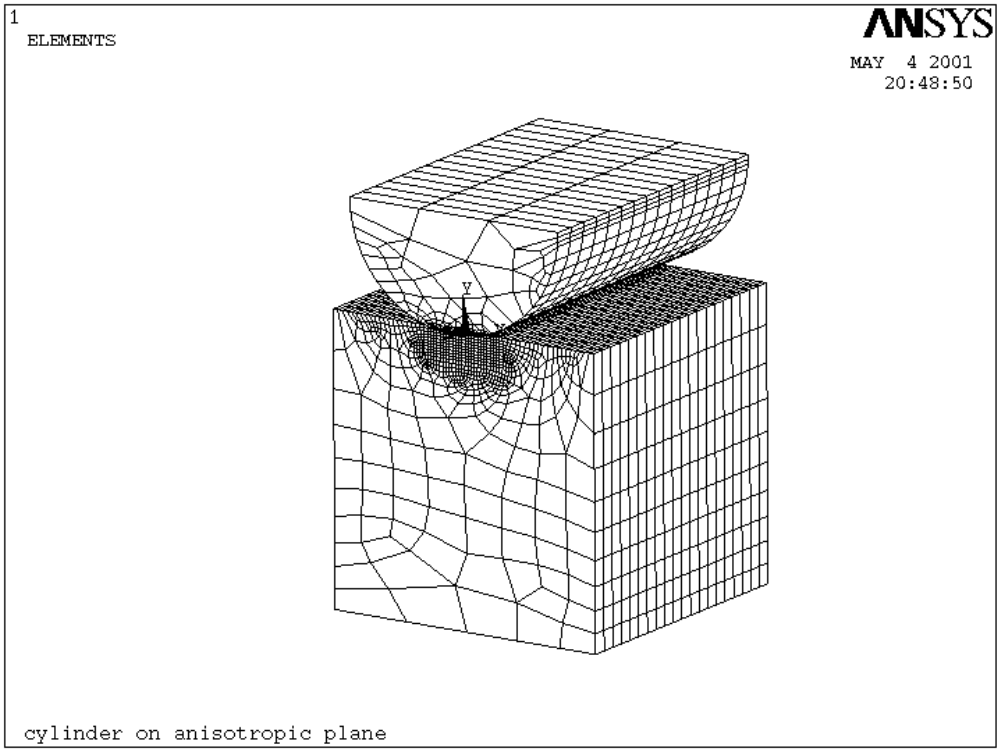

Figure 4 Finite element model of a cylinder on composites

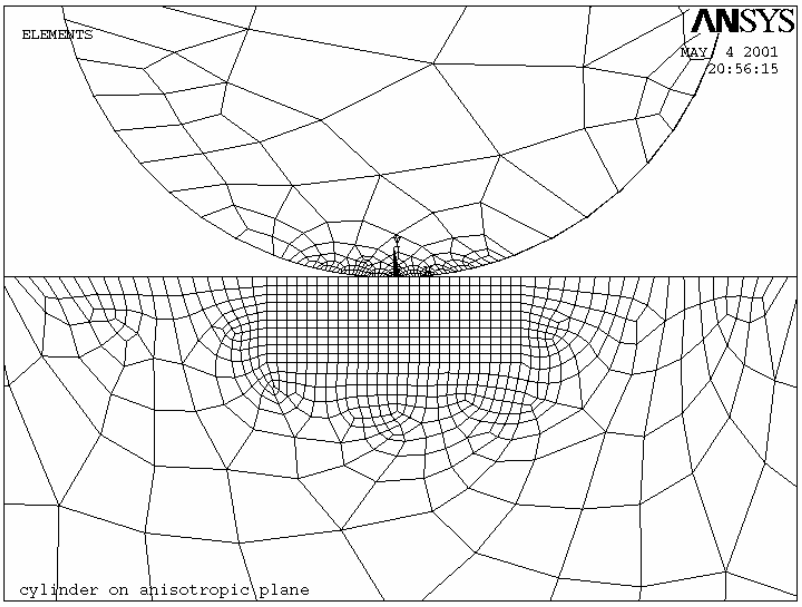

Figure 5 Finely meshed contact surface in x-y plane

Before these analytical solution results are related to the published experimental results, the analytical solution presented in this work will be initially evaluated with respect to results obtained from the finite element method. For the purpose of assessment, a three-dimensional finite element model was constructed to simulate a cylinder that slides with respect to a unidirectional continuous composite substrate. As illustrated in Fig.4, the model is generated using ANSYS®/LS-DYNA 5.7 and given boundary conditions to obtain results under the idealized condition of an infinitely long rigid cylinder that is in normal and tangential contact with a transversely isotropic half-plane. In the model, the half-plane was defined with material properties of Epoxy/T300 (density is 1536kg/m^3 and the cylinder was specified as a rigid. The half-plane was defined with dimension of 0.02m wide, 0.05m high, and 0.02m long and its displacement along the bottom surface were constrained in all three principal directions. The radius and length of the cylinder are 8 mm and 22 mm, respectively. Both the cylinder and half-plane were meshed using eight-node structural solid elements and the entire model consisted of 14320 elements for the fiber reinforced polymer composites and 3120 elements for the rigid cylinder. Finite element results were obtained in PL, TL, and NL orientations by varying the anisotropic material properties of the half-plane (see Table 2) and then applying normal load (1N/mm) and a sliding velocity (v=0.1 m/s) to the cylinder.

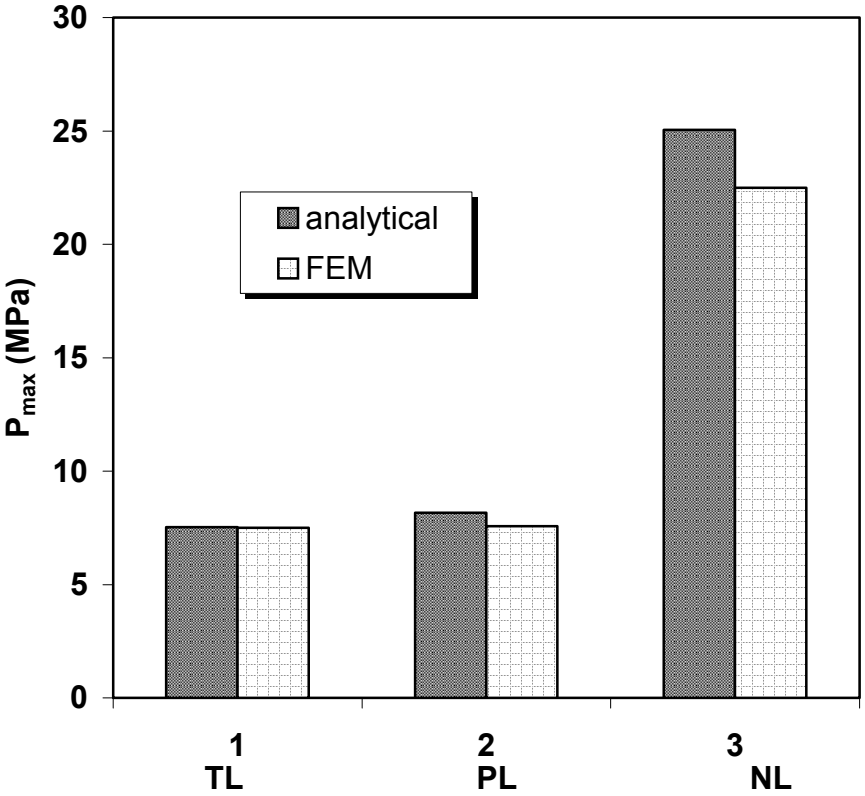

Figure 6 Comparison of analytical and numerical solutions

Comparing the analytical and numerical results, good correlation was found in all three fiber orientations. As illustrated in Fig.6, the differences in the maximum contact pressure predicted analytically and by the FEM are very small. In fact, the pressures vary by only 0.1 percent and 1.8 percent respectively in the TL and PL orientations. The largest difference between values is in the NL direction where the analytical and FEM results differ by 6.25 percent. The authors believe that this difference was due to approximations in the numerical model, and better correlation could have obtained by further refining the mesh of the half-plane in the contact region. Nonetheless, the small differences between the analytical and FEM results in all of the directions indicate that the present approach is valid for predicting the contact behavior of FRP composites.

In the literature, experimental research [2, 7] has indicated that the greatest wear resistance of FRP composites was obtained when the fiber alignment was normal to the sliding contact plane (normal orientation), and the lowest wear resistance occurred when the indenter crossed the fiber alignment (TL). These trends are similarly found using Hwu and Fan's solution and can be explained by combining asperity wear rate theory with the results of Fig. 3. In wear rate models of an asperity's indentation [8, 9], the wear rate has been shown to be directly proportional to the contact penetration and inversely proportional to the contact width. In addition to depicting the influence of fiber orientation on surface pressure, Fig. 3 can also be utilized to illustrate how the fiber orientation affects the wear in FRP composites. Prior research [7] has shown that FRP composites have three distinct wear mechanisms: (1) excess thinning of fibers, (2) fracture of fibers, and (3) peeling of fibers from the matrix. Under large penetrations, it is more likely for asperities to break fibers and peel them from the matrix. Since the

penetration is proportional to the size of the contact width, Fig. 3 shows that the cylinder produces the largest penetration in the transverse fiber orientation and the smallest in the normal fiber orientation. Therefore Eqs. 2.24-2.27 predict that the largest wear resistance occurs in the normal fiber orientation and the smallest resistance is obtained in the transverse fiber orientation, which is identical to the experimental results in [2, 7]. This correlation with the experimental results shows that the anisotropic theoretical approach utilized in this work may be used to gain information about the wear of FRP composites.

Table 2 Material Properties

FRP	Fiber			Matrix		
	Modulus (GPa)	**Poisson's Ratio**	**Frictional Coefficient**	**Modulus (GPa)**	**Poisson's Ratio**	**Frictional Coefficient**
Epoxy + Glass Fiber [8]	72	0.2	0.43	0.33	0.34	0.3
Epoxy + Aramid Fiber [7]	130	130	0.17			
Epoxy + Stainless steel [7]	186	0.3	0.18			
Epoxy + AS4 (Carbon fiber) [2]	235	0.2	0.2			

3.3.2 Influence Of Fiber Materials

With a large number of fiber materials available, it is important to establish how fiber material affects the contact behavior of FRP composites. Figs. 7-9 illustrate the variation of the pressure distributions of four different fiber materials in the transverse, normal and parallel fiber alignments, respectively. The fiber materials and their properties are given in Table 2. It is important to note that the polymer resin material was identical for all results in Fig. 7. Examining the figures, it is found that the variation of the fiber materials has little effect on the profile and magnitude of the pressure in the PL and TL directions. In the PL results of Fig. 9, it is found that the maximum normal pressure increases slightly from 43.9825 to 44.7381 MPa for the glass and carbon fibers respectively. For these fiber materials the value of δ increases from 0.489 to 0.4976 in the PL orientation, showing that the contact profile becomes more symmetric and decreases in magnitude (see Fig. 9) with increasing fiber elastic modulus.

Turning our attention to the transverse fiber orientation results in Fig. 7, it is similarly found that the fiber material has little influence on the contact profile. In fact, the contact pressure only increases from 40.86 MPa for the glass fiber to 41.3 MPa for carbon fiber, and there is negligible change in the area of the contact patch. There is however, a moderate increase in the symmetry in the contact patch between glass and carbon fibers, as δ was found to increase from 0.4569 to 0.4838.

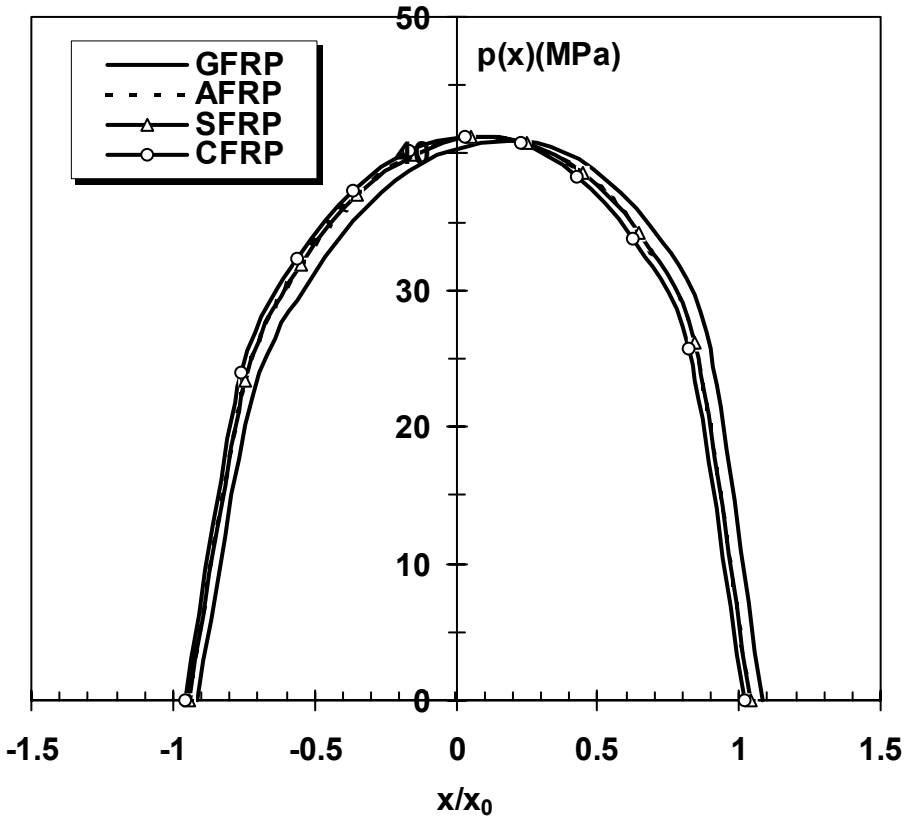

Figure 7 Pressure in transverse orientation for different fibers

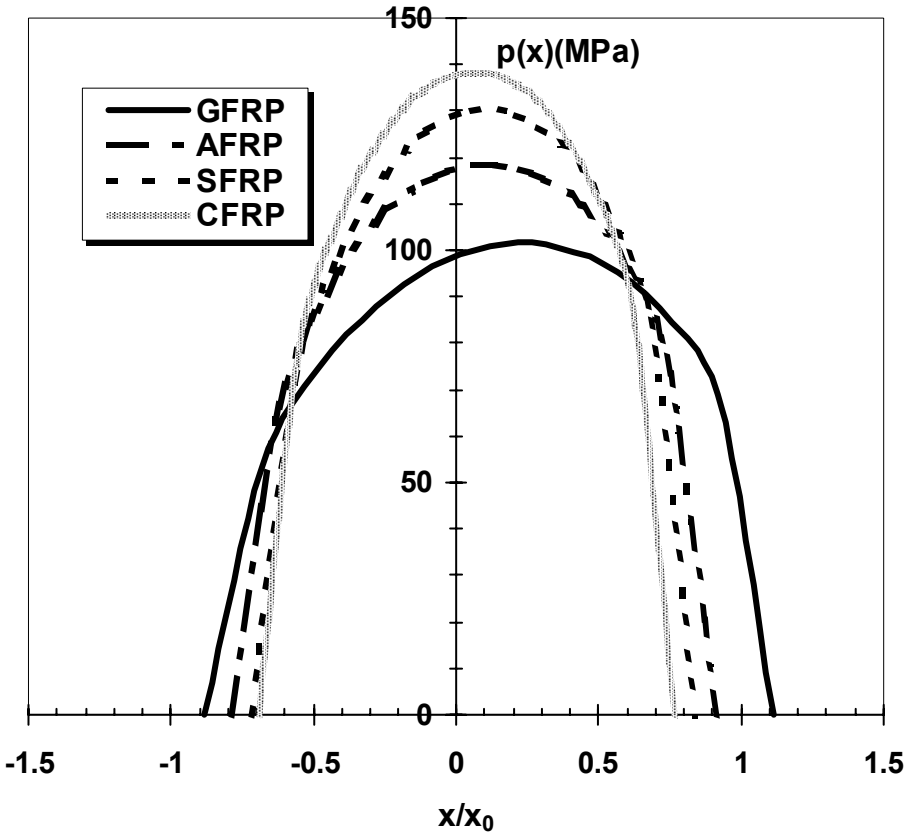

Figure 8 Pressure in normal orientation for different fibers

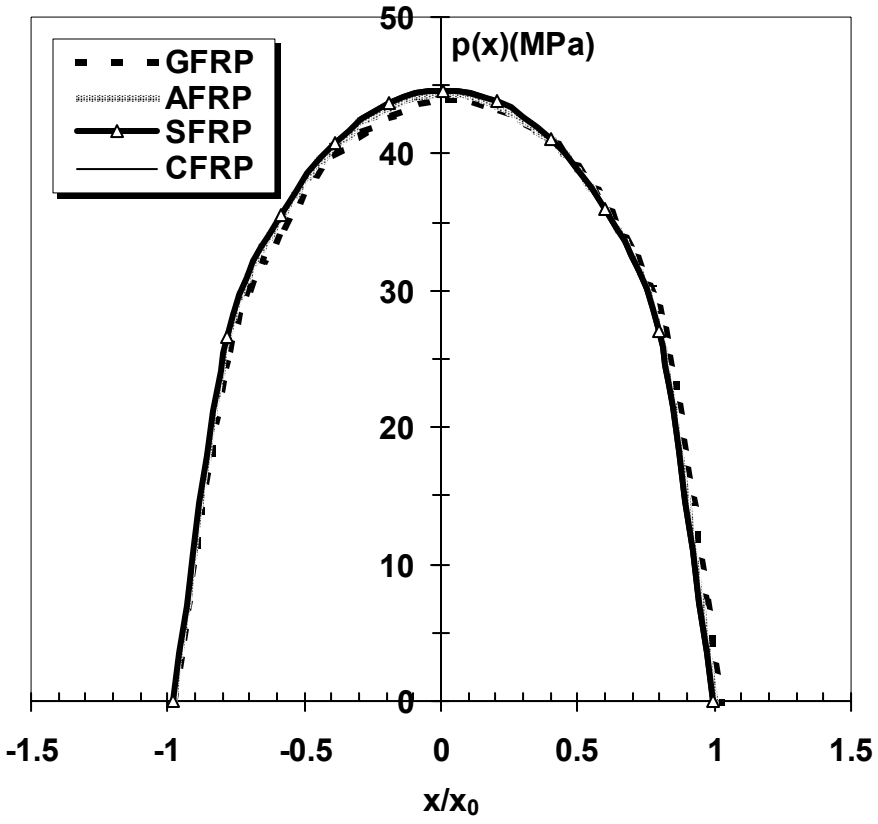

Figure 9 Pressure in parallel orientation for different fibers

In contrast with the variation of the pressure distributions in the PL and TL alignments, the pressure profile considerably changed with fiber materials in the NL orientation. As shown in Fig. 8, the contact width considerably narrows and the maximum pressure sharply increases with the longitudinal elastic modulus of the fiber. In the figure, the maximum contact pressure for epoxy/E-glass composites is approximately 101 MPa, whereas that for epoxy/AS4 composites is 138 MPa. It is also found in the figure that the maximum contact pressure in the normal fiber orientation becomes substantially more symmetric with an increased elastic modulus of the fibers, as δ for glass fibers is only 0.4416 while δ=0.4770 for the carbon fibers. These findings demonstrate that the contact traction in the normal fiber alignment has a great sensitivity to the variation of fiber material properties. Such a tendency can again be explained by the fact that fibers carry a significantly larger portion of the load in the normal orientation compared to the PL and TL orientations. Therefore, the stiffness and resultant pressure distribution is strongly influenced in the NL alignment by the material properties of the fibers.

3.3.3 Influence Of Fiber Volume Fractions

The fiber volume fraction of an FRP composite is a very important parameter in determining the composites stiffness characteristics. This is due to the fact that the engineering properties of a composite are often dominated by the mechanical and physical properties of the fiber reinforcement. Since the fiber material is generally several hundred times stiffer than its matrix counterpart, increasing the fiber volume fraction in an FRP composite will substantially decrease its compliance.

For the purpose of quantifying the influence of fiber volume fraction on the pressure distribution in FRP composites, Figs. 10-12 were generated for the three fiber alignments. In the figures, the fiber volume fraction was varied between 0.3 and 0.75 for an epoxy/E-glass FRP composite. As expected, Figs. 10-12 all show that the variation of fiber volume fraction has a considerable influence on the contact pressure distribution. As the volume of the filled fiber increases from 0.3 to 0.75, the maximum pressure values for all three principal fiber orientations approximately double. This indicates the prominent role that the fibers have in increasing the stiffness of the FRP composites. Likewise, the contact distribution becomes less symmetric as the fiber volume fraction increases, for example, in the TL orientation δ=0.4687, 0.4630, 0.4569, 0.4507 for the volume fractions of 0.30, 0.45, 0.60, 0.75. The significant variation of the contact properties with fiber volume fraction enables a designer to create FRP composites for a specific application. It is important to note, however, that there are limits on the magnitude of the fiber volume fraction, as the matrix volume fraction must be sufficient to satisfy its bonding and protective functions.

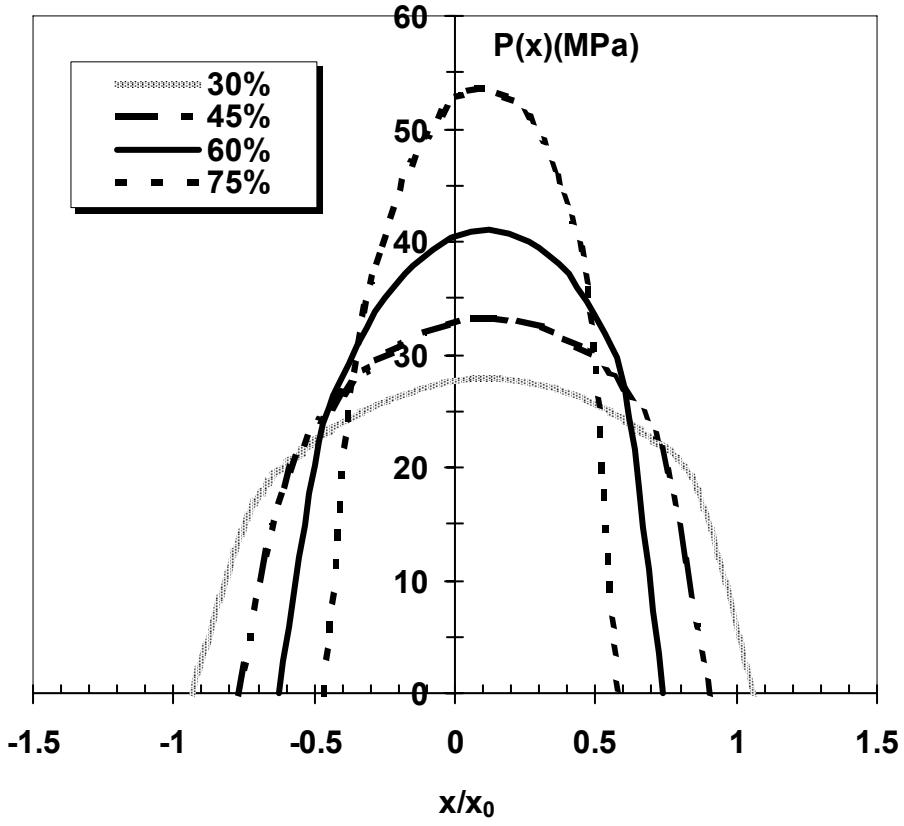

Figure 10 Pressure in transverse orientation for different fiber fractions

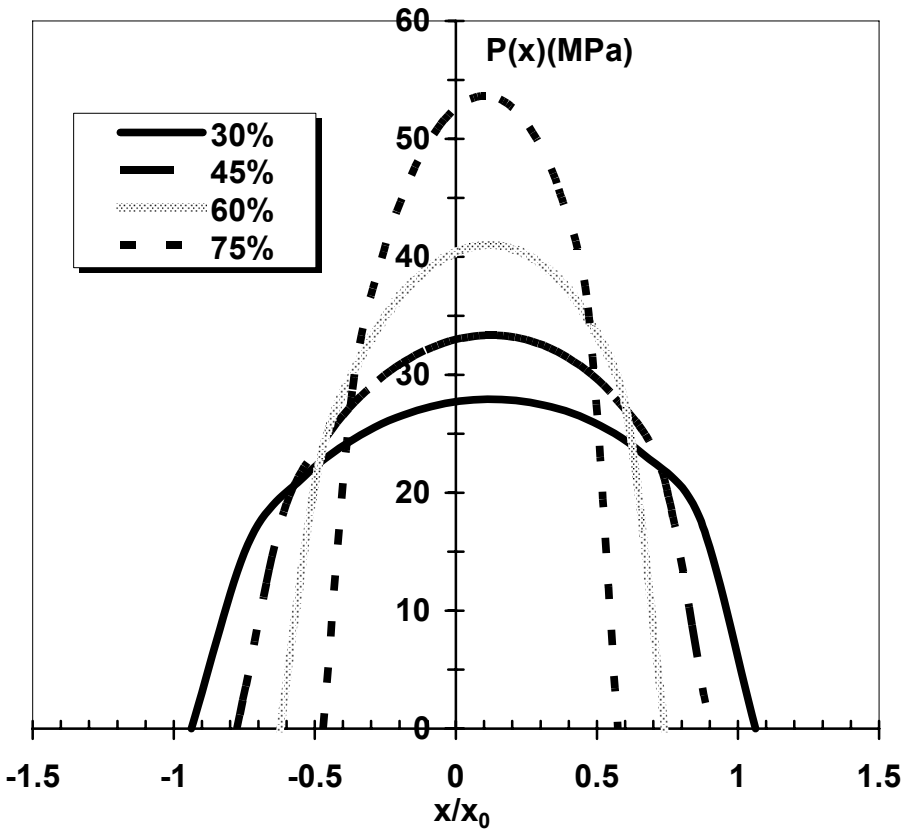

Figure 11 Pressure in normal orientation for different fiber fractions

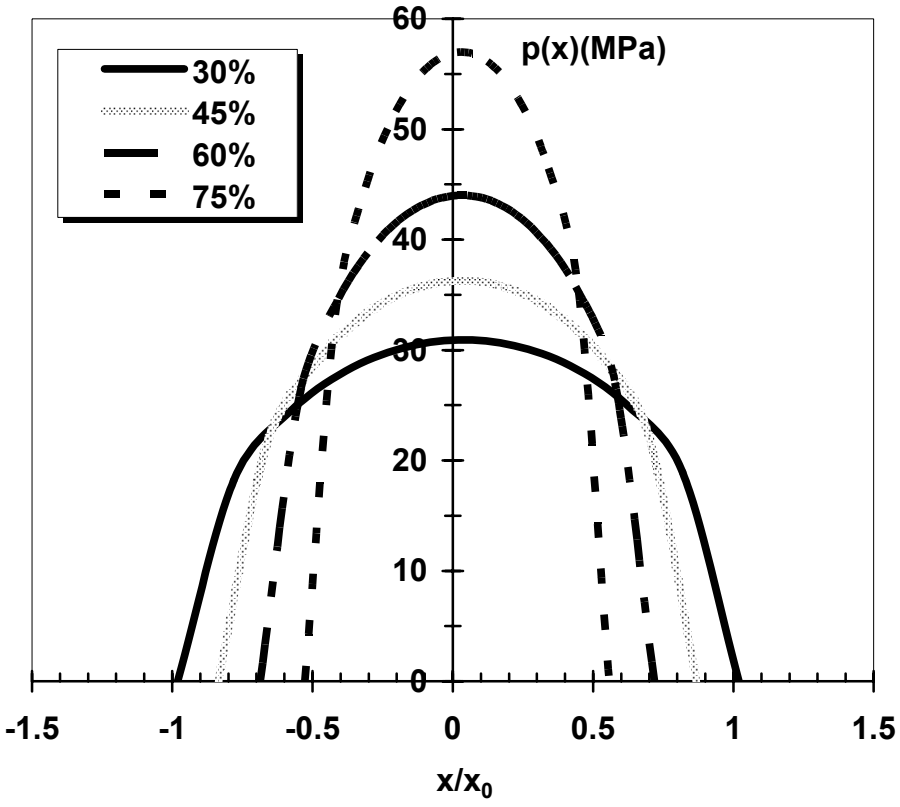

Figure 12 Pressure in parallel orientation for different fiber fractions

3.3.4 Influence Of Matrix Materials

Polymer resins are an essential part of FRP composites, as they serve as the bonding and protective agent for the reinforcing fibers. In addition to the strong influence of the fibers, the matrix material is an important factor in determining the contact behavior of FRP composites. In order to assess the role of matrix material on the pressure distribution, Figs. 13-15 were generated at the three orientations for resin materials of epoxy and PEEK. In the figures, the composites consist of AS4 carbon fibers with a fiber volume fraction of 60%. As shown in the figures, the matrix material has an important influence on the pressure distribution. In particular, the maximum pressure increases by 300% in the TL and PL alignments when the matrix material is changed from epoxy to PEEK. This is clearly due to the fact that the PEEK resin (E=3.6GPa) is much stiffer than the epoxy (E=0.33GPa) material, and therefore has a lower compliance as indicated by the smaller contact areas of Figs. 13-15. Considering the symmetry of the contact patch, all three orientations show that δ is moderately larger (δ_{TL}=0.4738 δ_{NL}=0.477, δ_{PL} =0.4976) for epoxy than for the stiffer PEEK resin material (δ_{TL}=0.448 δ_{NL}=0.4335, δ_{PL} =0.4805).

A final item that is interesting to note is that the properties of the matrix material has less influence in the NL direction than the TL and PL directions. As shown in Fig. 9b, the maximum pressure increases less than 100% between that epoxy and PEEK matrix materials. Considering that an increase of over 300% was found in the PL and TL orientations, it is again clear that the fibers reinforcements play a more significant role in carrying the load in the NL orientation.

Table 3 Material properties of PEEK/AS4 graphite FRP

FRP	Fiber		Matrix		Composites
PEEK + AS4 [4]	Modulus (GPa)	Poisson's Ratio	Modulus (GPa)	Poisson's Ratio	Frictional Coefficient
	235	0.2	3.6	0.30	0.4

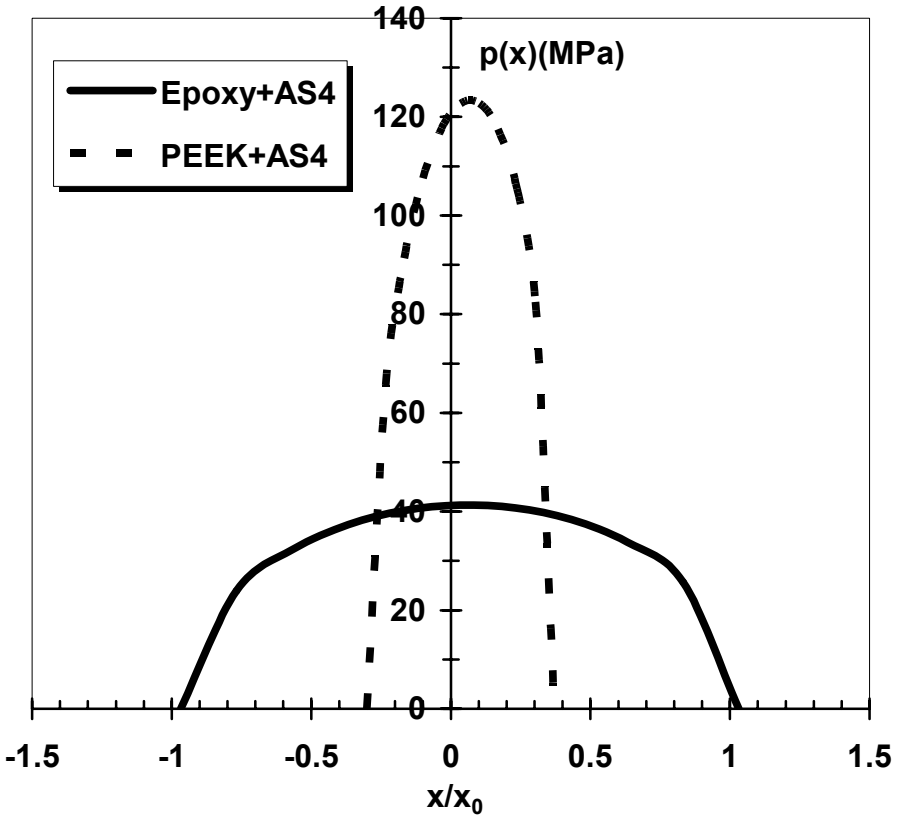

Figure 13 Pressure in transverse orientation for different matrices

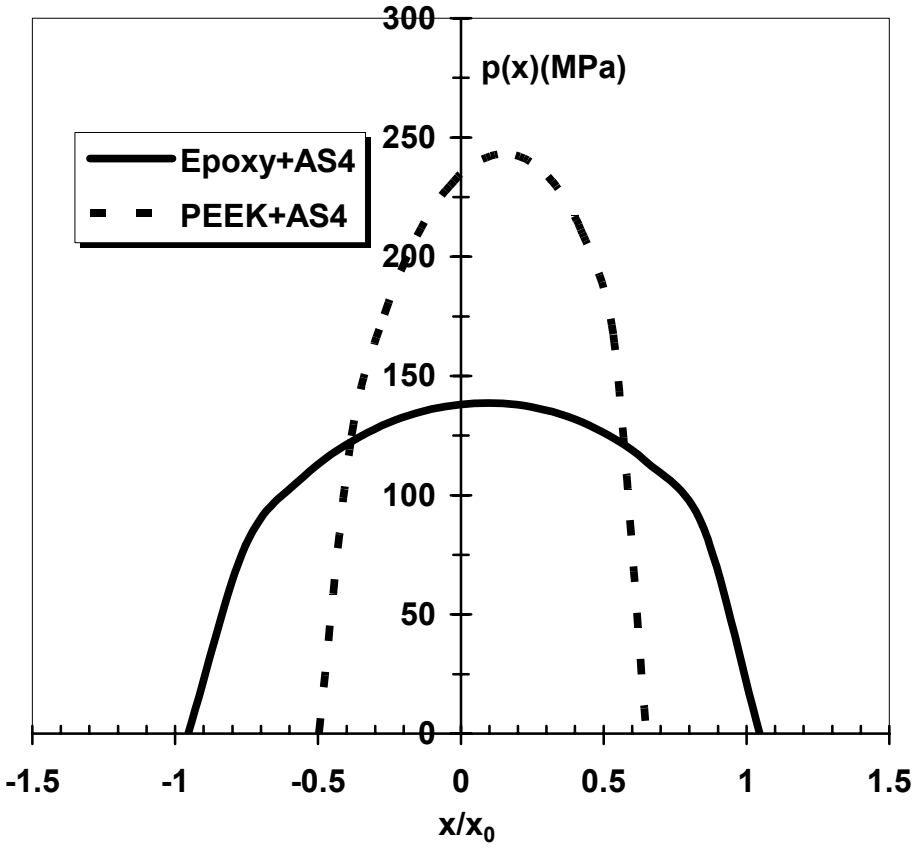

Figure 14 Pressure in normal orientation for different matrices

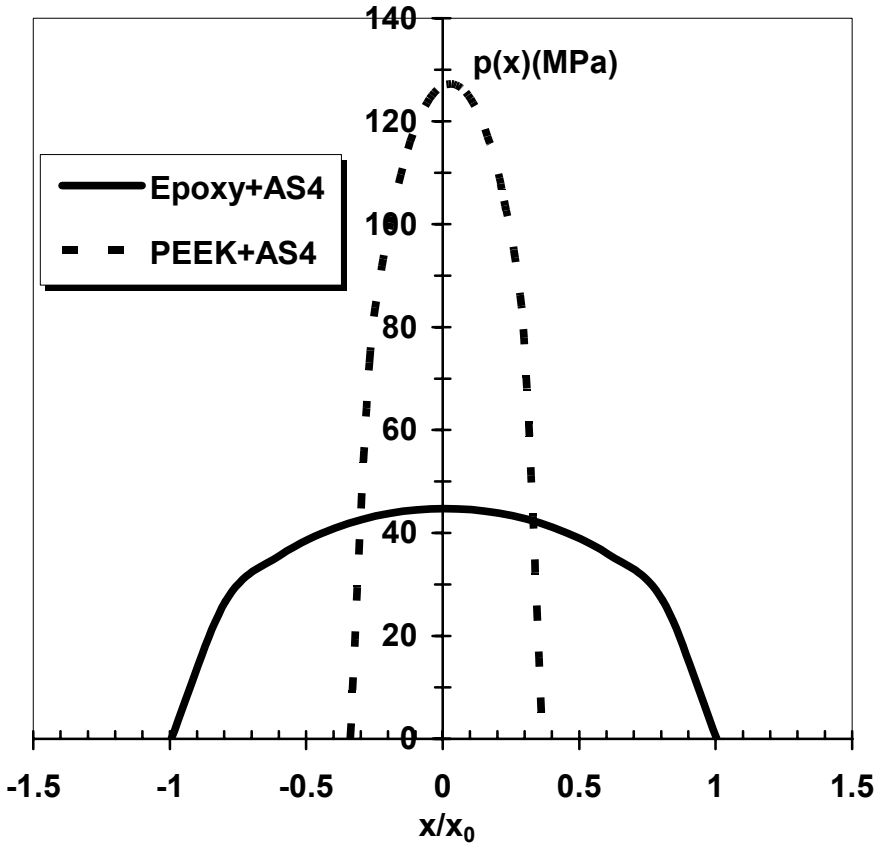

Figure 15 Pressure in parallel orientation for different matrices

3.3.5 Influence Of Friction Coefficient

The final parameter to be analyzed for the contact characteristics of FRP composites is the friction coefficient. Since the friction coefficient of composites depend on numerous factors including material constituents, fiber alignment, and surface roughness, the friction coefficient should be considered a parameter that can be adjusted to attain a desired effect. However, care should be taken, because increasing the frictional coefficient to high levels will lead to larger frictional forces, and experiments [7] have shown that wear rates dramatically increase with the frictional forces experienced by FRP composites. The overall influence of the friction coefficient on the pressure distribution of FRP composites in each of the three orientations is shown in Figs. 16-18. In the figures, the friction coefficient is varied between 0.15 and 0.75 for an epoxy/K-49 (Aramid) composite. As illustrated in the figures, the friction coefficient has a small effect on the maximum contact pressure and the contact area. When considering the symmetry of the contact area, however, the friction coefficient has a substantial influence in the TL and NL orientations. As the friction coefficient increases from 0.15 to 0.75, δ decreases from 0.4823 to 0.4135 in the TL orientation and from 0.4757 to 0.3836 in the NL orientation. Such a decrease in δ is expected, as increasing the friction coefficient tends to elongate the contact patch in the direction of sliding. It is very important to point out that a similar change in δ is not found in the PL alignment. In fact, Fig. 18 shows that the friction coefficient has virtually no influence on the contact pressure distribution in the PL alignment. Such a finding can be explained by the fact that the sliding of the cylinder in the PL alignment is parallel to the fibers, and therefore will not significantly increase the shear forces they experience.

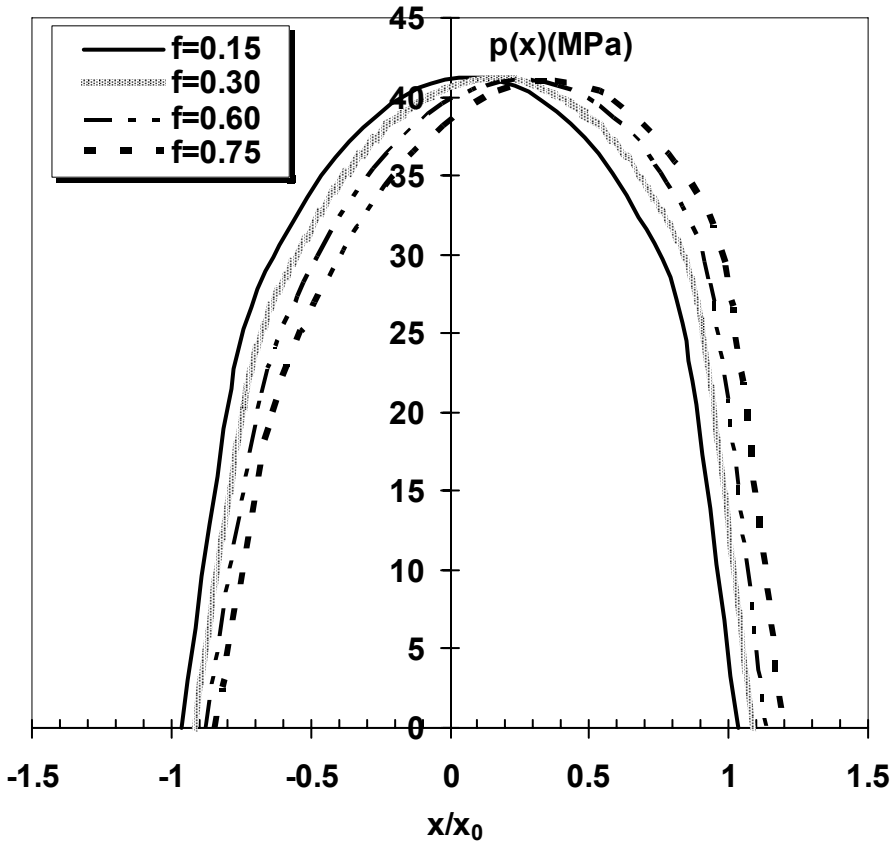

Figure 16 Pressure in TL for different friction coefficients

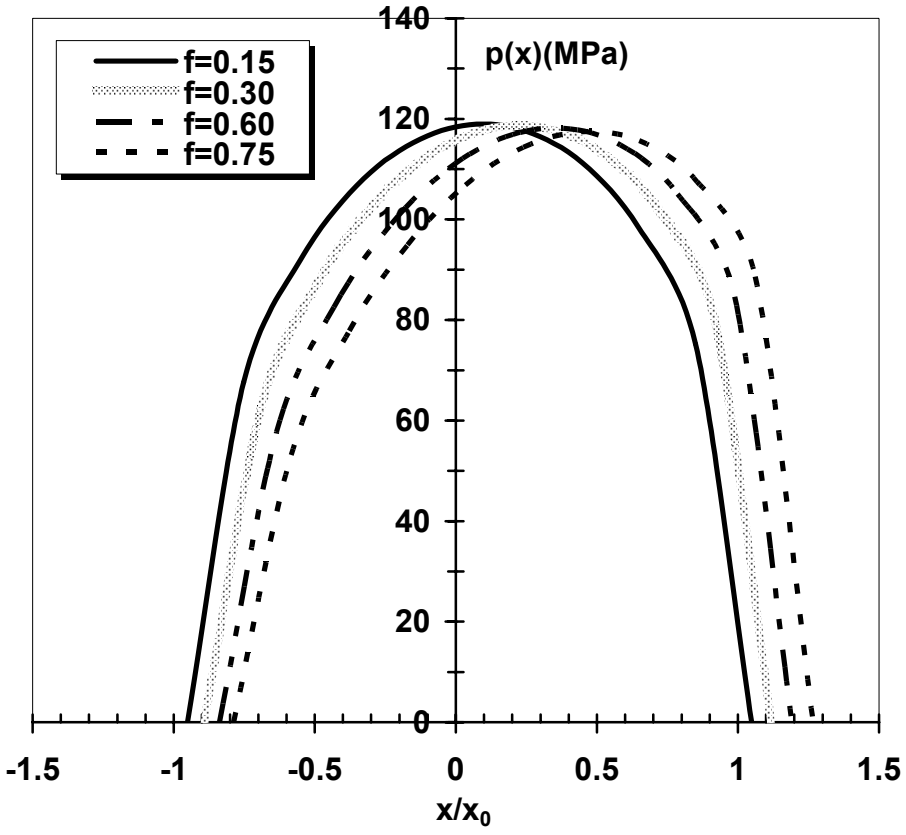

Figure 17 Pressure in NL for different friction coefficients

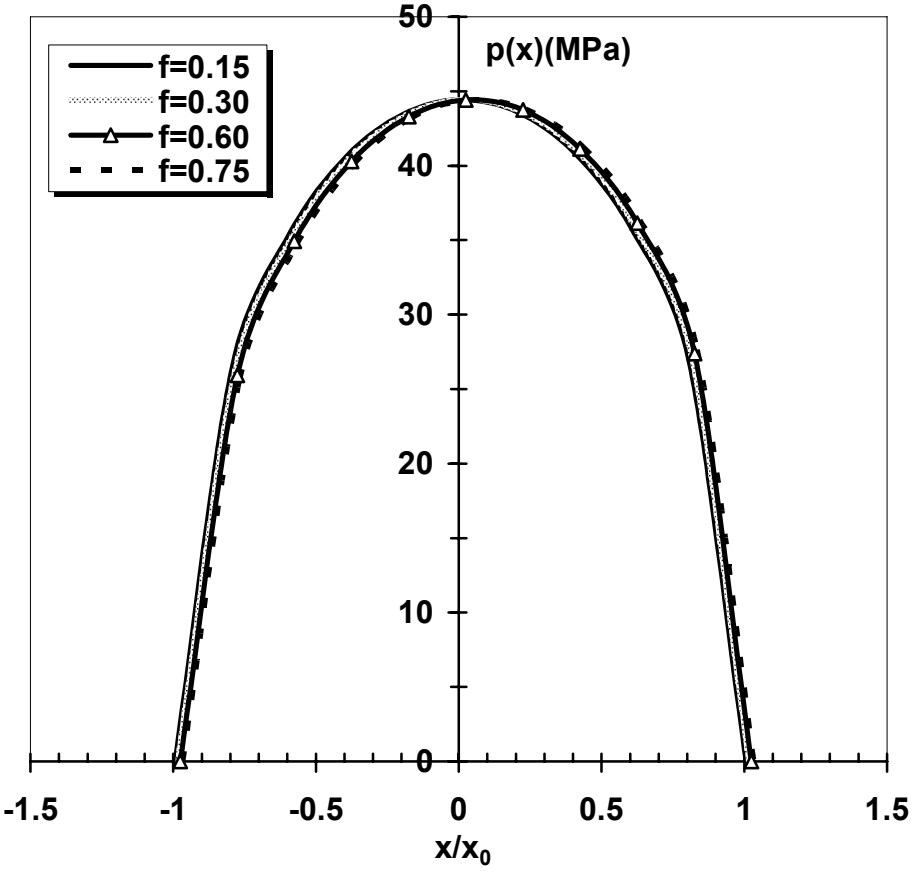

Figure 18 Pressure in PL for different friction coefficients

3.4 Conclusion

By applying a closed form sliding contact solution for an anisotropic half-plane, the effects of matrix material, friction coefficient, fiber material, fiber orientation and fiber volume fraction on the contact characteristics of FRP composites have been evaluated. The trends determined for this analytical approach was found to match very closely with published experimental results. From the analytical data, several important tendencies for FRP composites have been determined, as related to optimizing the tribological performance of FRP materials. These findings are summarized below:

- The highest maximum contact pressure was obtained in the normal fiber orientation, and the lowest maximum contact pressure was obtained in the transverse fiber orientation. The large contact pressure in the NL orientation was due to the fibers carrying a large portion of the load.
- The analytical results indicated that the contact penetration and contact patch play critical roles in the wear of FRP composites. Therefore, similar to that found by experiments [2, 3, 7], the NL fiber orientation possesses the highest wear resistance.
- The friction sliding pressure distributions of FRP materials were not symmetrical, as the maximum contact pressure is inclined to the sliding direction. The contact pressure distribution in the normal fiber alignment has the least symmetric contact area, whereas the parallel fiber alignment is the most symmetric.
- With a variation of fiber materials, the contact pressure in the transverse and parallel fiber orientations shows little change. In the normal fiber alignment, however, fiber materials significantly influence the contact behavior. This trend was attributed to the

fact that the fibers carry a substantial portion of the normal load in the NL direction, and therefore is more sensitive to fiber material properties.

- Since fibers are several hundred times stiffer than matrix materials, increasing the fiber volume fraction of FRP composites increases the maximum contact pressure in all the three fiber alignments.
- The elastic modulus of the matrix material also has a strong influence on the maximum contact pressure distribution. The normal orientation was least sensitive to changes in matrix materials.
- The frictional coefficient of FRP composites has little influence on the magnitude of the contact pressure in all the three fiber orientations. The magnitude of the friction coefficient did have a significant influence on the symmetry of the contact patch, except for the PL orientation.

4.0 CONTACT BEHAVIOR IN ARBITRARY FIBER ORIENTATIONS

In the above section, the sliding occurs in the principal orientations of orthotropic materials. If the sliding is along the arbitrary fiber orientations, composites demonstrate the off-axis elastic properties and the Barnett-Lothe tensors cannot be obtained through Eqs. 3.3-3.7. In this section, the contact behavior is investigated by incorporating the numerical solutions of the explicit expressions of Barnett-Lothe tensors and the off-axis elastic properties.

4.1 Off-Axis Elastic Properties Of Composites

The arbitrary sliding directions with respect to the fiber alignment may be expressed with the current Cartesian coordinate system rotating about the origin. The direction cosines between the current coordinate axes, X', Y', Z' and the original coordinate axes, X, Y, Z are l_1, m_1, n_1, l_2, m_2, n_2, l_3, m_3, n_3, respectively. The current off-axis elastic properties C' are given by:

$$C' = ACA^T \tag{4.1}$$

where A is the transformation matrix shown below:

$$A = \begin{bmatrix} l_1^2 & m_1^2 & n_1^2 & 2m_1n_1 & 2n_1l_1 & 2l_1m_1 \\ l_2^2 & m_2^2 & n_2^2 & 2m_2n_2 & 2n_2l_2 & 2l_2m_2 \\ l_3^2 & m_3^2 & n_3^2 & 2m_3n_3 & 2n_3l_3 & 2l_3m_3 \\ l_2l_3 & m_2m_3 & n_2n_3 & m_2n_3+m_3n_2 & n_2l_3+n_3l_2 & l_2m_3+l_3m_2 \\ l_3l_1 & m_3m_1 & n_3n_1 & m_3n_1+m_1n_3 & n_3l_1+n_1l_3 & l_3m_1+l_1m_3 \\ l_1l_2 & m_1m_2 & n_1n_2 & m_1n_2+m_2n_1 & n_1l_2+n_2l_1 & l_1m_2+l_2m_1 \end{bmatrix} \tag{4.2}$$

When the axes of the coordinate system do not coincide with the material principal axes, the transversely isotropic material may become triclinic materials (without symmetry plane), or monoclinic materials (with one symmetry plane).

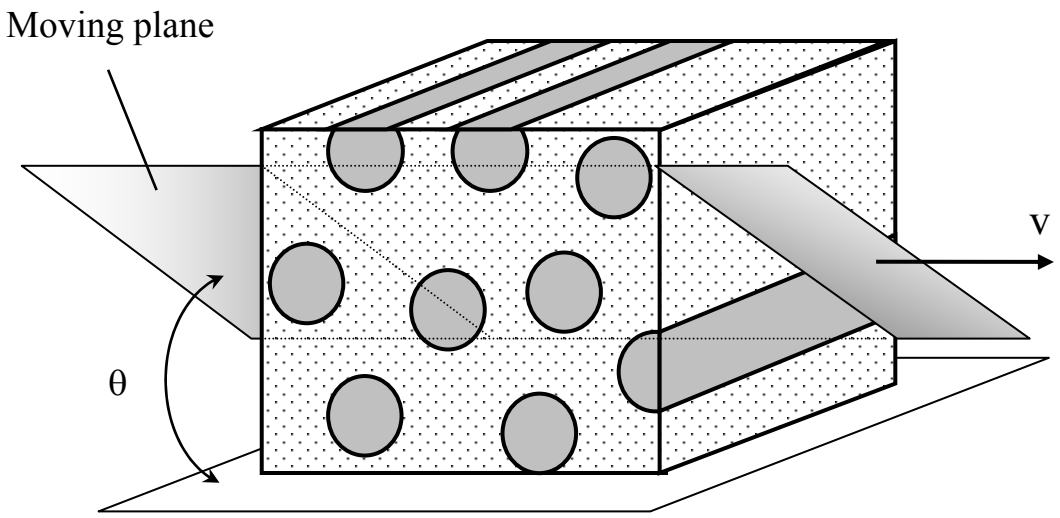

Figure 19 Transition of fiber orientations from TL (θ=0deg) to NL (θ=90deg)

4.2 Explicit Expression Of Barnett-Lothe Tensors

For generally anisotropic materials, Yin [39] obtained the explicit expressions of Barnett-Lothe tensors.

Firstly, define three matrices:

$$Q=\begin{bmatrix} C_{11} & C_{16} & C_{15} \\ C_{16} & C_{66} & C_{56} \\ C_{15} & C_{56} & C_{55} \end{bmatrix},\ R=\begin{bmatrix} C_{16} & C_{12} & C_{14} \\ C_{66} & C_{26} & C_{46} \\ C_{56} & C_{25} & C_{45} \end{bmatrix},\ T=\begin{bmatrix} C_{66} & C_{26} & C_{46} \\ C_{26} & C_{22} & C_{24} \\ C_{46} & C_{24} & C_{44} \end{bmatrix} \tag{4.3}$$

where $[C_{ij}]$ is the elastic constants of generally anisotropic materials.

Define a matrix with the above three matrices as follows:

$$\Pi = Q + \omega(R + R^T) + \omega^2 T \tag{4.4}$$

where ω is the eigenvalues of matrix $\prod$, superscript T represents transpose. There are three cases for the explicit expressions of Barnett-Lothe tensor, as demonstrated by [39]:

- If the equation $\prod(\omega)=0$ has three distinct roots ω_j (j=1, 2, 3), the materials are called N-simple materials. For N-simple materials**:**

$$L = -2i\sum_{j=1}^{3}[1/\Omega'(\omega_j)(R^T + \omega_j T)\hat{\Pi}(\omega_j)(R + \omega_j T)] \tag{4.5}$$

$$S = -2i\sum_{j=1}^{3}[1/\Omega'(\omega_j)\hat{\Pi}(\omega_j)(R+\omega_j T)] + iI \tag{4.6}$$

- If the equation $\prod(\omega)=0$ has one simple root ω_1 and one double root ω_2, the materials are called N-double materials. For N-double materials:

$$\begin{aligned} L = -2i[&\{1/\Omega'(\omega_1)\}(R^T+\omega_1 T)\hat{\Pi}(\omega_1)(R+\omega_1 T) \\ &+(2/\Omega''(\omega_2))[(R^T+\omega T)\hat{\Pi}(\omega)(R+\omega T)]'(\omega_2) \\ &+(2/3)(1/\Omega''(\omega_2))'(R^T+\omega_2 T)\hat{\Pi}(\omega_2)(R+\omega_2 T)] \end{aligned} \tag{4.7}$$

$$\begin{aligned} S = -2i[&\{1/\Omega'(\omega_1)\}\hat{\Pi}(\omega_1)(R+\omega_1 T) \\ &+(2/\Omega''(\omega_2))[(R^T+\omega T)\hat{\Pi}(\omega)(R+\omega T)]'(\omega_2) \\ &+(2/3)(1/\Omega''(\omega_2))'\hat{\Pi}(\omega_2)(R+\omega_2 T)] + iI \end{aligned} \tag{4.8}$$

- If the equation $\prod(\omega)=0$ has a triple root ω, the materials are called N-triple materials. For N-triple materials (extra-degenerate case):

$$\begin{aligned} L = -&\{6i/\Omega'''(\omega)\{(R^T+\omega T)\hat{\Pi}(R+\omega T)\}'' \\ &-3i(1/\Omega''')'\{(R^T+\omega T)\hat{\Pi}(R+\omega T)\}' \\ &+(6i/19)(1/\Omega''')''(R^T+\omega T)\hat{\Pi}(R+\omega T) \end{aligned} \tag{4.9}$$

$$\begin{aligned} S = -&\{6i/\Omega'''(\omega)\{\hat{\Pi}(R+\omega T)\}'' \\ &-3i(1/\Omega''')'\{\hat{\Pi}(R+\omega T)\}' \\ &+(6i/19)(1/\Omega''')''(\hat{\Pi}(R+\omega T)+iI \end{aligned} \tag{4.10}$$

where $\hat{\Pi}(\omega)$ represents the adjoint matrix of $\prod(\omega)$, I is a unit matrix. $\Omega(\omega)$ is the determinant of $\prod(\omega)$, $(\,)'$ represents a derivation, $i=\sqrt{-1}$.

Incorporate above explicit expression of Barnett-Lothe tensors, the characteristic parameters β and δ may be determined.

4.3 Solutions And Discussion

The contact pressure distribution in FRP composites can be calculated from the representation of the elastic properties (Eqs. 4.1-4.2), the analytical solutions (Eqs. 2.24-27), and the relationship (Eqs. 2.28-2.29) between the contact parameters and the Barnett-Lothe tensors (Eqs. 4.5-4.10). The calculation procedure involves the numerical solution of a sixth-order linear Eq. 4.4 to obtain the eigenvalues and the eigenvector for the explicit expression of the Barnett-Lothe tensors.

It is important to verify the numerical results obtained with the above procedure. Since there are the analytical expressions of Barnett-Lothe tensors for orthotropic materials [15], the contact results may be obtained for three principal fiber orientations without solving the sixth-order equation (Eq. 4.4) and using the explicit expressions of Barnett-Lothe tensors (Eqs.4.5-4.10). By the comparison of the results for the NL, the TL and the PL, the present program for generally anisotropic materials give the same results as those [8] by the means of the analytical expression when the applied load is the same.

Three special cases will be considered in this work: (i) the fiber orientation as it rotates from the transverse fiber orientation (TL) to the parallel direction (PL); (ii) the fiber orientation as it rotates from the transverse fiber orientation (TL) to the normal direction (NL); (iii) the fiber orientation as it rotates from the parallel fiber orientation (PL) to the normal direction (NL). Fig. 19 shows the transition of the fiber orientation from the TL to the NL. It is assumed that a moving plane may cut through the composites from left to right and slide relative to the stationary composite. The angle between the moving plane and horizontal is indicted by θ. In the figure, changing the angle transitions the fiber orientation from the TL (θ=0deg) alignment to the

NL (θ=90deg) orientation. The former two cases involve both in-plane and out-plane deformations, while the last case only experiences in-plane deformations. The materials corresponding to the three cases are classified as monoclinic materials, i.e., ones with one symmetry plane.

In order to demonstrate the applicability of the analytical method presented in this work, a unit normal line force (F=1 N/mm) and an indenter radius of 8 mm will be evaluated for one of the most common FRP composites, epoxy/T300 (Table 1). The analytical results are plotted in Figs. 20-22 where the maximum pressure, parameter δ, and the contact patch width are respectively plotted as a function of the fiber orientation.

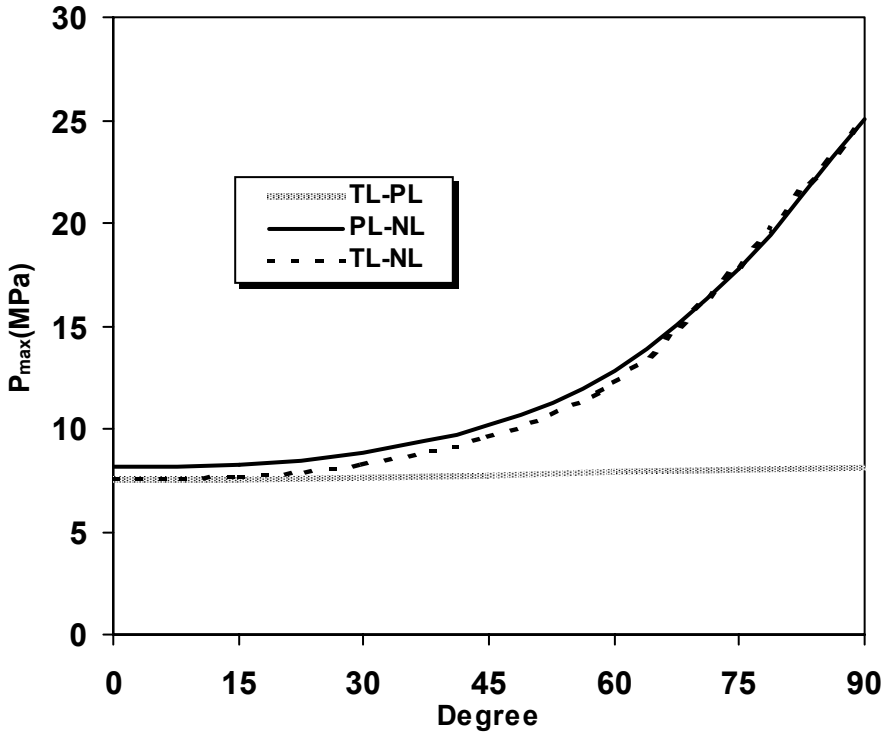

Figure 20 Variation of the maximum pressure P_{max} with the fiber orientation

Examining Fig. 20, it is found that the maximum contact pressure distribution monotonically varies with the fiber orientation. Closely examining the figure, the smallest maximum pressure is obtained when the sliding contact occurs in the transverse (TL) fiber alignment, while the largest maximum pressure occurs in the normal (NL) fiber orientation. In addition, the maximum pressure in the parallel orientation (PL) is only slightly higher than in the TL. Comparing the pressure values in the TL and the NL directions, it is found that the maximum pressure increases by more than 300% when the fiber orientation rotates from the TL to the NL orientations. An identical trend is also shown when the fiber orientation varies from the PL to the NL orientations. This can best be explained by considering the stiffness variability of FRP composites in different directions. In the NL fiber orientation, the composites demonstrate a high stiffness because the fibers carry the largest portion of the load and their elastic modulus is large. This is in contrast to the TL and the PL orientations where the composites possess a relatively small stiffness. In fact, since there is only a slight increase in the stiffness as the contact orientation rotates from the TL to the PL alignment, little variation in the maximum contact pressure occurs. Hence, it can be concluded that the elastic stiffness of the composites in the normal contact direction plays a predominant role in determining the maximum contact pressure.

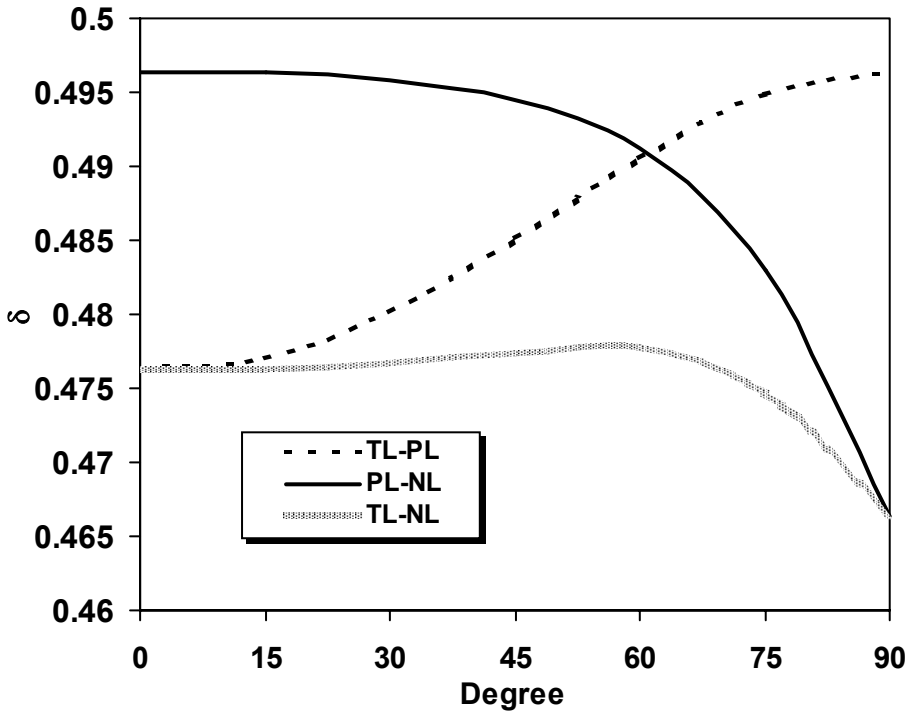

Figure 21 Variation of δ with the fiber orientation

Turning our attention to the contact area, the symmetry of the contact patch can be characterized by the ratio of the contact patch dimensions a/b. As described previously, the parameter δ also describes the geometrical characteristics of the contact pressure profile. The relationship between δ and a/b may be obtained by combining Eqs. 2.26 and 2.27:

$$\delta = \frac{a/b}{a/b+1} \tag{4.11}$$

The influence of fiber orientation on the symmetry of the contact patch is depicted in Fig. 21. As shown in the figure, the value of δ substantially decreases as the fiber orientation rotates from the PL to the NL direction, increases as the orientation rotates from the TL to the PL direction, and non-monotonically varies as the orientation rotates from the TL to the NL direction. The value of δ in the NL orientation is 0.4663, which is the smallest among the three principal fiber orientations. This indicates the maximum contact pressure in the NL alignment deviates the farthest distance from the vertical axis of the cylinder. Conversely, the value of δ in the PL alignment is the highest at 0.4964, which shows that the maximum contact pressure is nearly symmetrical. Such trends demonstrate the important role that the fiber orientation has in determining the asymmetry of the contact area.

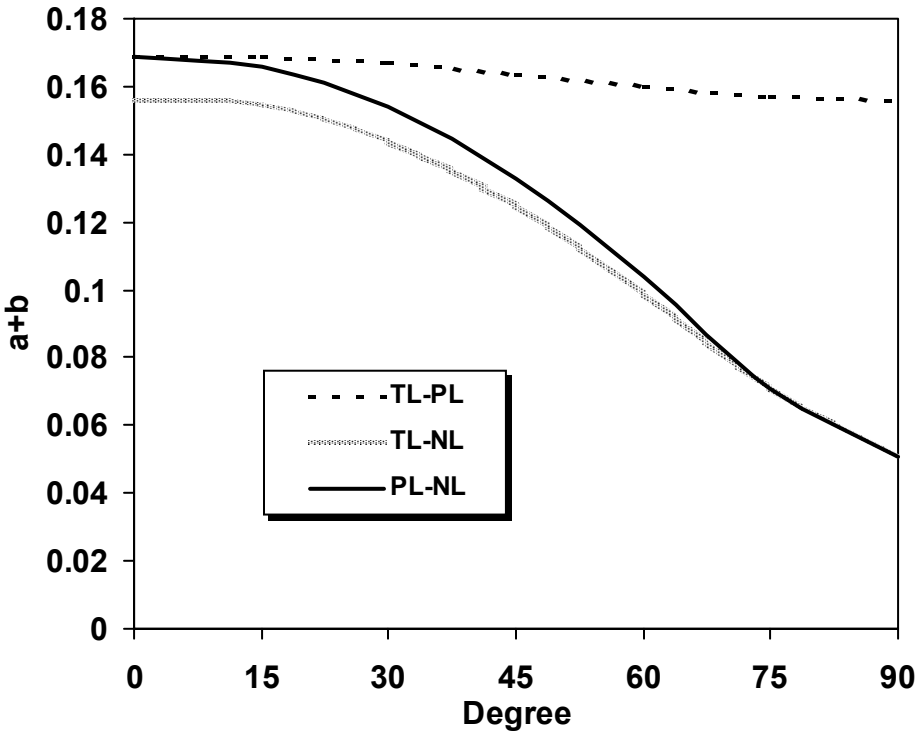

Figure 22 Variation of contact patch width with the fiber orientation

As shown in the Fig. 22, the total contact width, $a+b$, is the smallest in the NL orientation. This can again be explained by the fact that the elastic stiffness in the contact direction plays a predominant role in determining the contact area. Therefore, as fiber orientation rotates from either the TL or PL orientation to the NL orientation, the contact width is found to decrease by more than 50% as the stiff fibers carry a larger portion of the load. As the fiber orientation rotates from the PL to the TL there is only slight decrease of the contact width.

It is interesting to note that the NL orientation, with the smallest contact area, is the most sensitive to friction. In the PL direction, sliding occurs along the direction of the fibers where composites have the largest stiffness. As a result, the PL orientation demonstrates the most symmetry, and is the least sensitive to the friction. In the TL orientation, the sliding crosses the fibers, and therefore the contact area will be less symmetric than in the PL direction. It can be concluded that the elastic stiffness in the sliding direction determines the sensitivity of the contact area to the friction.

The relevance of studying the contact behavior of FRP composites lies within the fact that the contact characteristics have substantial influence on the wear performance. Prior research [7] has shown that the wear of FRP composites is a fiber-dominated process as the failure most commonly occurs in the form of excess thinning of fibers, fracture of fibers, and peeling of fibers from the matrix. These three wear mechanisms are all directly related to the deformation or the strain in the contact region. The contact deformation may be taken as the resultant response of the anisotropic elastic material when it is subjected to the contact loading. Under large deformations, it is more likely for the fibers to break and peel from the matrix. Since the contact penetration is proportional to the size of the contact width, Fig. 22 shows that the cylinder produces the largest penetration in the transverse fiber orientation and the smallest in the

normal fiber orientation. The penetration in the parallel orientation is slightly narrower than in the transverse. From the viewpoints of the contact deformation, it can generally be concluded, as indicated in previous experimental research [2,3,7], that the largest wear resistance was obtained when the fiber alignment was normal to the sliding contact plane (NL), although the wear resistance in the TL and PL cannot be determined by the contact deformation.

Since the variation of the contact width is monotonically as the fiber orientation varies from the TL or PL direction to the NL orientation, or from the TL to PL orientation, the tendency for wear for some composites like T300/Epoxy can be deduced from the contact width curves in Fig. 22. For example, the wear rate when the fiber orientation rotates from the TL to the NL should be lower than the wear rate in the TL, but larger than that in the NL direction. In fact, this conclusion is in exact agreement with the experimental data of Sung and Suh [2] on epoxy/T300 when the fiber orientations varied from the TL to the NL. This correlation with the experimental results shows the real contact area plays a very important role in the wear of unidirectional continuous FRP composites. It should be noted, however, that the wear of FRP composites is a complicated process involving thermal, chemical and coupled field effects, so that the geometrical deformation only accounts for the mechanical effect. Lhymn [3] employed the microstructures of PAN carbon fiber morphology to explain the difference of the friction and wear behavior between the TL and PL

4.4 Conclusion

By incorporating the explicit expression of Barnett-Lothe tensors to a closed-form sliding contact solution for an anisotropic half-plane, the anisotropic contact behavior of FRP composites has been investigated. Several trends for the tribological performance of FRP materials have been ascertained and discussed. These trends are summarized below:

- The maximum contact pressure and contact width of FRP composites are dominated by the elastic stiffness in the normal contact direction, and therefore the largest maximum contact pressure and the smallest contact area occur as the sliding direction is rotated to the NL orientation.
- The maximum contact pressure and the contact width were found to monotonically vary as the fiber orientation was rotated between PL, NL, and TL orientations.
- Based on the comparison with the experiment data, the level of contact deformation in FRP composites was found to correlate with the wear rate.
- The contact symmetry parameter δ was found to be highly dependent on the fiber orientation.

5.0 DEVELOPMENT OF WEAR MODEL FOR FRP COMPOSITES

5.1 Wear Analysis

Wear is closely correlated with failure stresses for isotropic materials because the wear process involves plastic yielding and deformation. It has been summarized by numerous researchers (cf. [43]) that there are three main contributions to wear: adhesion, abrasive, and asperity deformation. Abrasive and adhesive wear are the two primary mechanisms for most ductile isotropic materials. For these materials, the wear rate may be expressed in the form [44]:

$$\dot{w} = k\frac{F}{H} \tag{5.1}$$

where k is the abrasive/adhesive wear constant factor; F is the applied force; and H is the material hardness. k, describing the probability that the material loses as wear debris, is dependent on materials. The hardness, defined as the applied load divided by the projected indentation area, is a measure of the plastic deformation in the contact region. The relationship between the hardness and the yield strength for isotropic materials has been given by Johnson [29]:

$$H = 2.8Y \tag{5.2}$$

The yield stress Y in Eq. 5.2 may be obtained according to von Mises shear strain energy criterion or Tresca's plastic criterion. Eqs. 5.1 and 5.2 demonstrate the quantitative relationship between wear and the failure strength.

The adhesive and abrasive wear mechanisms have similarly been found in anisotropic FRP composites [2]. The wear of FRP composites, however, cannot be characterized directly in terms of Eqs. 5.1-5.2 because the von Mises yield criterion cannot be applied to FRP composites due to the anisotropy. In addition, the above equations do not include the influence of the fiber orientation on the wear. As observed on their worn surfaces [7], the wear modes of fiber-reinforced composites are a fiber-dominated process, which involves fiber fracture, fiber pullout, matrix crack, and fiber and matrix thinning. With the exception of the fiber and matrix thinning, all of the above wear modes are similar to the micro-scale failure modes of the fibrous composites. Hence, it is prudent to assume that the anisotropic failure criteria can be employed to characterize the wear of fiber-reinforced composites.

5.2 Anisotropic Strength Approach

There are several widely applied biaxial strength criteria for fiber-reinforced composites [45, 46]. These criteria include: (1) maximum stress failure criterion; (2) maximum strain failure criterion; (3) Tsai-Hill failure criterion; (4) Hoffman failure criterion; (5) Tsai-Wu failure criterion. Since the Tsai-Wu failure criterion has exhibited the best agreement with FRP composites experimental data, superior curve-fitting capability, and a convenient mathematical operation, it will be employed in the present investigation to develop an analytical model for anisotropic wear. It should be noted that the Tsai-Wu strength criteria provides a tool to curve-fit failure data for FRP composites, but does not reveal which failure modes occur. This is similarly true for all the above failure strength criteria that predict the failure but do not indicate a specific failure mechanism.

The application of a macro-scale anisotropic failure criteria implicitly requires that the wear of FRP composites satisfy two hypotheses:

- The composites are homogeneous.
- The contact and wear behavior of composites results from the averaged or mixed constituent material properties in a direction.

In general, the above two assumptions are well conceived because the wear performance largely depends upon the bulk mechanical properties of materials. In this case, FRP composites may be assumed quasi-homogeneous and anisotropic.

The Tsai-Wu failure criterion is a quadratic tensor polynomial criterion that includes linear terms [47]. Tsai-Wu assumed that a scalar function $\Delta(\sigma_i)$ exists in the form [46]:

$$\Delta(\sigma_i) = \Gamma_i \sigma_i + \Gamma_{ij} \sigma_i \sigma_j \qquad i, j = 1, \ldots 6 \tag{5.3}$$

where Γ_i and Γ_{ij} are strength tensors of the second and fourth rank, respectively. Failure occurs under the conditions:

$$\Delta(\sigma_i) \geq 1 \tag{5.4}$$

Considering the orthotropic composites under plane stress conditions, the criterion Eq. 5.4 is expressed by the failure surface [46]:

$$\Gamma_1 \sigma_1 + \Gamma_2 \sigma_2 + \Gamma_6 \sigma_6 + \Gamma_{11} \sigma_1^2 + \Gamma_{22} \sigma_2^2 + \Gamma_{66} \sigma_6^2 + 2\Gamma_{12} \sigma_1 \sigma_2 = 1 \tag{5.5}$$

$$\Gamma_1 = \frac{1}{X_t} + \frac{1}{X_c} \tag{5.6}$$

$$\Gamma_2 = \frac{1}{Y_t} + \frac{1}{Y_c} \tag{5.7}$$

$$\Gamma_{11} = -\frac{1}{X_t X_c} \tag{5.8}$$

$$\Gamma_{22} = -\frac{1}{Y_t Y_c} \tag{5.9}$$

$$\Gamma_6 = 0 \tag{5.10}$$

$$\Gamma_{66} = \frac{1}{S_s^{\,2}} \tag{5.11}$$

$$\Gamma_{12} = \frac{1}{2\sigma^2}\left[1 - \left(\frac{1}{X_t} + \frac{1}{X_c} + \frac{1}{Y_t} + \frac{1}{Y_c}\right)\sigma + \left(\frac{1}{X_t X_c} + \frac{1}{Y_t Y_c}\right)\sigma\right] \tag{5.12}$$

where X and Y are the failure strength in the principal axes 1 and 2 and the subscripts t and c represent tension and compression respectively. In Eq. 5.5, $\sigma_6 = \tau_{12}$, S_s is the shear strength, and σ is the biaxial tensile failure stress. Because it is difficult to obtain a reliable value of Γ_{12} through experiments and there is little influence of Γ_{12} on the overall results, Narayanaswami and Adelman [48] suggested that Γ_{12} be taken as zero. As a result, Eq. 5.5 may be transformed to a standard ellipsoidal equation of the form:

$$\frac{(\sigma_1 + \frac{\Gamma_1}{2\Gamma_{11}})^2}{d_1^2} + \frac{(\sigma_2 + \frac{\Gamma_2}{2\Gamma_{22}})^2}{d_2^2} + \frac{\tau_{12}^2}{d_3^2} = 1 \tag{5.13}$$

$$d_1^2 = \frac{1 + \frac{\Gamma_1^2}{4\Gamma_{11}} + \frac{\Gamma_2^2}{4\Gamma_{22}}}{\Gamma_{11}} \tag{5.14}$$

$$d_2^2 = \frac{1 + \frac{\Gamma_1^2}{4\Gamma_{11}} + \frac{\Gamma_2^2}{4\Gamma_{22}}}{\Gamma_{22}} \tag{5.15}$$

$$d_3^2 = \frac{1 + \frac{\Gamma_1^2}{4\Gamma_{11}} + \frac{\Gamma_2^2}{4\Gamma_{22}}}{\Gamma_{66}} \tag{5.16}$$

The space formed by $\sigma_1 - \sigma_2 - \tau_{12}$ is an ellipsoid. It is symmetric about the shear stress plane so that $\tau_{12} = 0$. Since the sign of the shear stress has no influence on the results, a semi-

ellipsoidal failure stress envelope can be generated as shown for Glass/Epoxy (Table 1) in Fig. 23. It should be noted that the scales of the three axes in Fig. 23 were made different for clarity. An identical scale for each axis would make the ellipsoid more slender and longer than that shown in Fig. 23. Such an ellipsoid constructs a yield surface, which covers possible failure stress states. A very slender and long failure envelope indicates that the strength of fiber-reinforced composites is highly anisotropic and is strongly a function of the fiber alignment. Continuous unidirectional FRP composites typically possess larger strengths in the longitudinal fiber alignment than in the transverse alignment. In general, the ellipsoidal failure stress envelope is not symmetrical about the plane $\sigma_1 = 0$ or $\sigma_2 = 0$. In the longitudinal fiber alignment, composites have larger maximum tension failure stress magnitudes than the compressive values. Conversely, the transverse fiber alignment of composites has a larger maximum compressive failure stress magnitude than a tension magnitude. It should be noted that the direction transverse to the fiber longitudinal orientation in a plane stress condition actually represents both fiber orientations, i.e., PL and TL. Thus, examining Fig. 23, the largest failure stress was obtained in the NL direction, while the lowest failure stress was in the PL or TL directions.

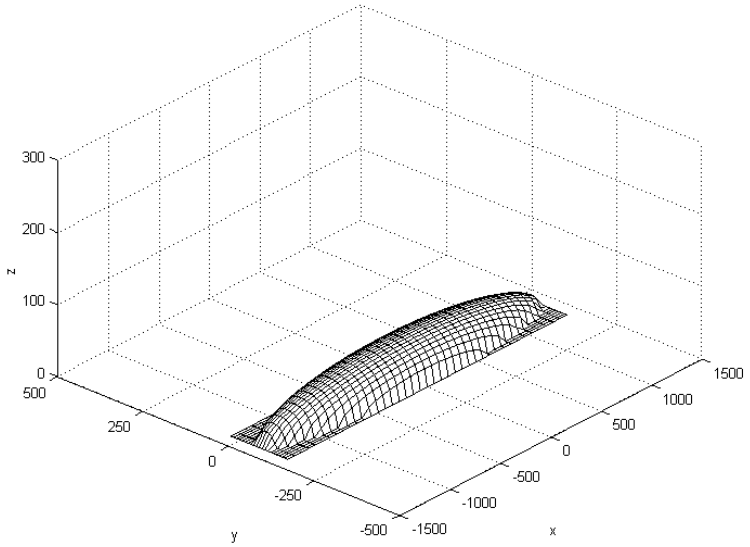

Figure 23 Ellipsoidal failure stress envelope for Glass/Epoxy: x, y –longitudinal, transverse principal stresses, respectively; z-shear stress

Considering a point within the centerline of the contact surface of the composites, the principal stresses σ_1 and σ_2 are compressive in nature. Therefore, the stress state will be enveloped within the third quadrant of the yielding surface. When subjected to the compressive stresses, the third quadrant in Fig. 23 predicts that the compressive failure stress decrease dramatically as the fiber orientation varies from the normal direction (NL) to the parallel or transverse direction (PL/TL). It also indicates that the NL orientation possesses the highest compressive strength. From this viewpoint, it is not surprising that experiments find that the wear varies with the fiber orientations and the largest wear resistance is obtained in the normal fiber orientation [2].

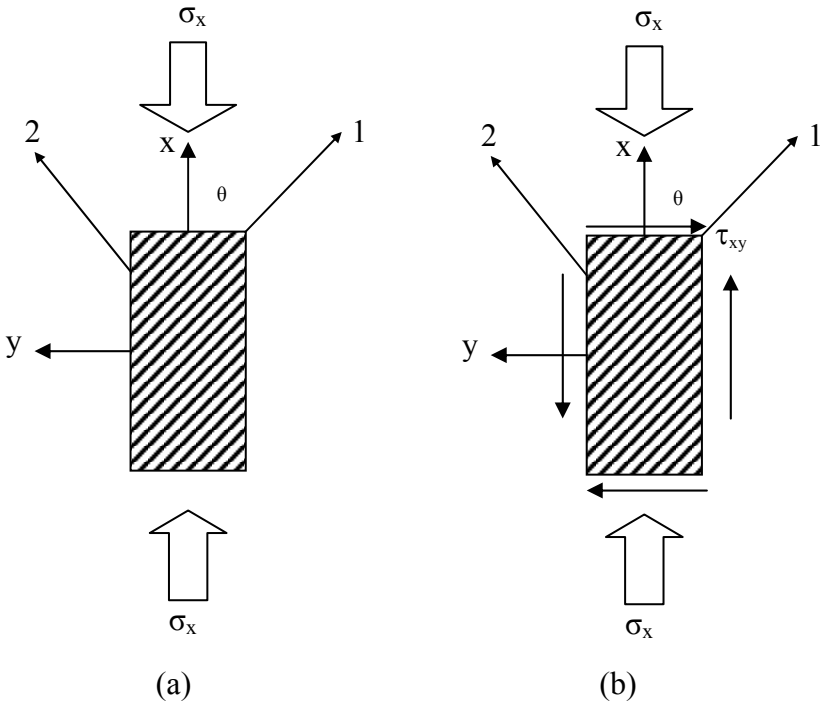

Figure 24 Biaxial stresses (a) off-axis uniaxial loading; (b) off-axis biaxial loading

The relationship between the fiber orientation and the strength can be further understood by transforming the results. The relationship between the stresses in the principal material coordinate system and those in the global coordinate system is:

$$\sigma_1 = \sigma_x \cos^2\theta + \sigma_y \sin^2\theta + 2\tau_{xy} \sin\theta\cos\theta \tag{5.17}$$

$$\sigma_2 = \sigma_x \sin^2\theta + \sigma_y \cos^2\theta - 2\tau_{xy} \sin\theta\cos\theta \tag{5.18}$$

$$\tau_{12} = -\sigma_x \sin\theta\cos\theta + \sigma_y \sin\theta\cos\theta + 2\tau_{xy} \cos 2\theta \tag{5.19}$$

For the special case of an off-axis coupon under uniaxial compressive stress, as shown in Fig. 24, the Tsai-Wu criterion takes a quadratic form when Eqs. 5.13-5.19 are combined:

$$\alpha\sigma_x^2 + \eta\sigma_x - 1 = 0 \tag{5.20}$$

where α and η are parameters expressed in the terms of the failure strengths and the fiber orientation θ :

$$\alpha = \xi^4\left(\frac{-1}{X_t X_c}\right) + \zeta^4\left(\frac{-1}{Y_t Y_c}\right) + \frac{\xi^2\zeta^2}{S_s^{\,2}} \tag{5.21}$$

$$\eta = \xi^2\left(\frac{1}{X_t} + \frac{1}{X_c}\right) + \zeta^2\left(\frac{1}{Y_t} + \frac{1}{Y_c}\right) \tag{5.22}$$

where $\xi = \sin\theta,\ \zeta = \cos\theta$. For given materials with known strengths, the failure stress σ_x can be solved as a function of θ. Fig. 25 shows how the compressive strength of three typical tribological FRP composites (Table 4) varies with the fiber orientation from the NL to PL/TL.

Table 4 Strength of FRP composites

FRP [46]	$\mathbf{X_t}$ (MPa)	$\mathbf{X_c}$ (MPa)	$\mathbf{Y_t}$ (MPa)	$\mathbf{Y_c}$(MPa)	$\mathbf{S_s}$ (MPa)
Glass/Epoxy	1035	1035	28	138	41
Graphite/Epoxy	1035	689	41	117	69
Kevlar/Epoxy	1380	276	28	138	44

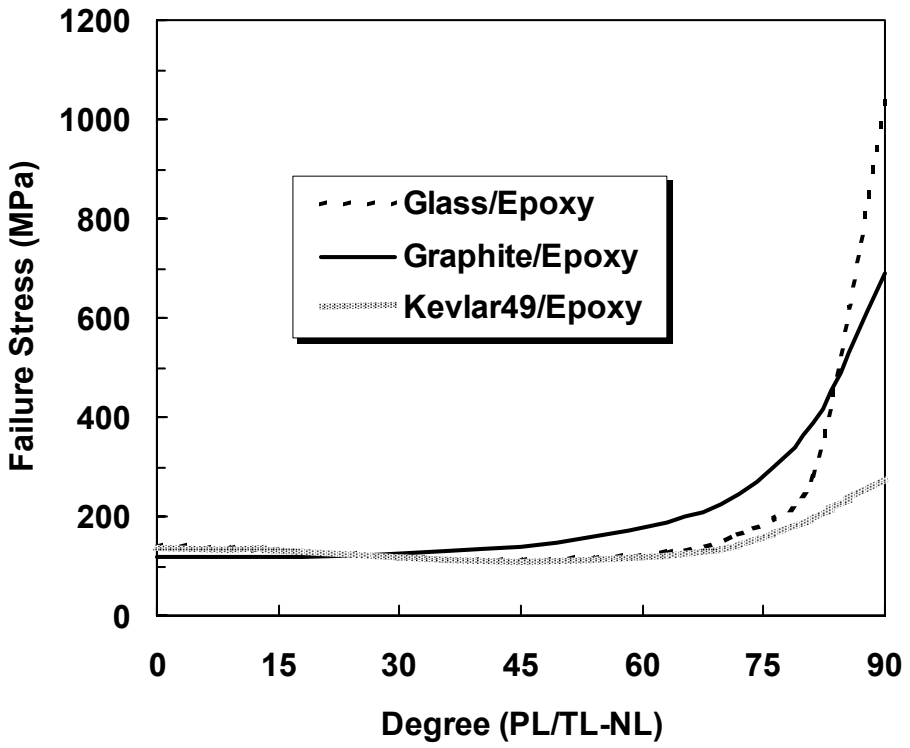

Figure 25 Failure compressive stress σ_x vs. fiber orientation from PL/TL to NL

Another important result that can be deduced from Eqs. 5.17-5.19 is the influence of the friction conditions on the failure strength. In order to elucidate the effect of friction, the case where there is no stress in the horizontal direction of the composites is considered, i.e.:

$$\sigma_y = 0 \tag{5.23}$$

Hence, when the composites are under the compressive and friction shear stresses shown in Fig. 24(b), the friction shear stress is:

$$\tau_{xy} = f\sigma_x \tag{5.24}$$

where f is the frictional coefficient. Similarly to Fig. 25 where friction was included, the compressive strength for T300/Epoxy (Table 1) is show in Fig. 26. Table 1 [2] lists the strength values of T300/epoxy that were used in the analytical calculations. Since the transverse compressive strength data was not given in the original literature [2], it was assumed that the transverse compressive strength of T300/Epoxy was -120 MPa. This assumption was based on data available for similar Graphite/Epoxy given in the literature [46]. In Fig. 26, it is shown that the friction coefficient has significant influence on the failure strength when the fiber orientation is near the NL alignment. When the friction coefficient is large, the maximum strength does not occur at the NL orientation, whereas it occurs near the NL orientation. It indicates that when the friction coefficient is small, the damage mode at the NL fiber orientation is governed by the compressive strength in the fiber orientation; when the friction coefficient is large, the failure

mechanism is dominated by the shear strength and transverse compressive strength. In the empirical wear rate Eq. 1, the wear is assumed to be proportional to the friction coefficient. Here, the friction loading is implicitly included in the failure strength as a nonlinear term. With the relationships between the strength and the fiber orientations established, an anisotropic wear model may be tentatively constructed so as to quantify the wear of fiber-reinforced composites.

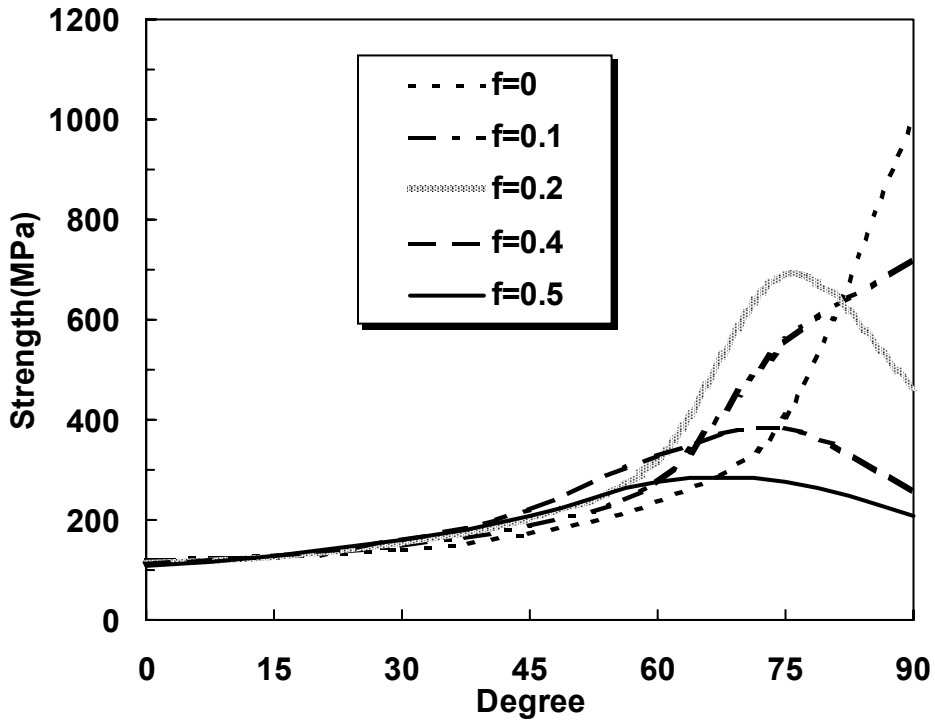

Figure 26 Compressive stress σ_x vs. fiber orientation from PL/TL to NL for T300/Epoxy

5.3 Development Of Wear Model

Wear rate is a complex function of loading conditions, material properties, and interface characteristics. An empirical wear rate equation should not only curve-fit the experimental data at reasonable accuracy, but also explain the wear phenomena. In this work, an anisotropic wear rate equation will be constructed based on the following two physical criteria:

- In a fiber orientation, the greater the failure strength, the less the wear.
- In a fiber orientation, the greater the stress, the more the wear

Using the above two conditions as a premise, the following first-order anisotropic wear model is proposed:

$$\dot{w}^{(\theta)} = k \frac{P_{\max}^{(\theta)}}{\sigma_x^{(\theta)}} \tag{5.25}$$

where $\dot{w}$ is the wear rate; k is a composite material wear factor; P_{max} is the maximum contact stress, varying with fiber orientations; σ_x is the failure compressive stress; and the superscript (θ) indicates the an arbitrary fiber orientation. The physical meaning of this model represents the probability that material loss occurs. In Eq. 5.25, the maximum contact pressure replaces the applied load in the original abrasive or adhesive model Eq. 5.1. The maximum contact pressure is used because the contact behavior of fiber-reinforced composites is anisotropic and the same loading may lead to different contact stress levels in different fiber orientations. In general, the maximum contact pressure in the NL orientation is several times that in the TL. Based on Eq. 5.25, the wear of fiber-reinforced composites can be theoretically predicted and investigated.

Compared to Eqs. 1.1 and 5.1, the wear model in Eq. 5.25 offers the following beneficial features:

- It is an anisotropic and includes anisotropic stress and strength.
- The friction condition is implicitly included in the strength.
- The contact behavior is expressed in terms of the maximum contact pressure, which is a function of the directional elastic properties of composites and the external loading. Eq. 1.1 only considers a single Young's modulus of the composites.

5.4 Comparison With Experimental Data

A theoretical predication of wear for T300/epoxy is listed in Table 6 as a function of the fiber orientation as it varies from the TL to the NL orientation. It is important to note that the composite material in the model is in a plane stress state as shown in Fig.27, the elastic constants is transformed as below:

$$c'_{ij} = c_{ij} - c_{i3}c_{j3}/c_{33} \tag{5.26}$$

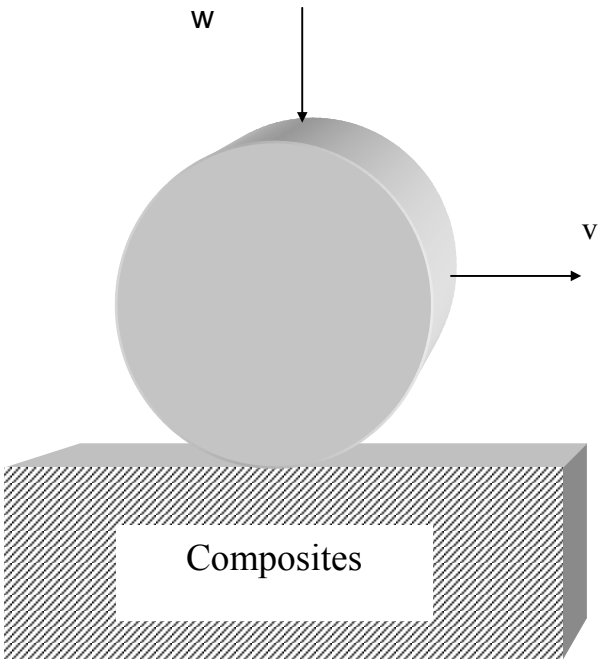

Figure 27 Schematic model of plane stress

Since the wear factor is dependent on materials, it can be used to construct a method to verify the wear model in Eq. 5.25 because k should be constant for a specific material. According to Eq. 5.25, the wear factor is:

$$k = \left(\dot{w}^{(\theta)}\right)_{test} \Big/ \left(\frac{P_{\max}^{(\theta)}}{\sigma_x^{(\theta)}}\right)_{theoretical} \tag{5.27}$$

In Eq. 5.27, the wear factor equals to the ratio of the test wear data over the theoretical values, $\dot{w}/(P_{\max}/\sigma_x)$. If Eq. 5.25 accurately predicts the wear rate for a specific material, the ratios of test wear data over the theoretical values, $\dot{w}/(P_{\max}/\sigma_x)$, should be equal for different fiber orientations, i.e.:

$$k_{\theta_1} = k_{\theta_2} = ... = const. \tag{5.28}$$

Therefore, in order to examine the above relationship (Eq. 5.28), the wear factors for T300/Epoxy are shown in Table 6 and Fig. 29. It is found that the ratios for the four fiber alignments are close to a constant, which is between $0.55\times10^{-7}$and 1.39×10^{-7} cm^3 kg^{-1} m^{-1}. The mean value of the wear factor for T300/Epoxy is 1.13×10^{-7} cm^3 kg^{-1} m^{-1}. Hence, it can be concluded that Eq. 5.25 may predict the wear rate from the TL to the NL at rather reasonable accuracy.

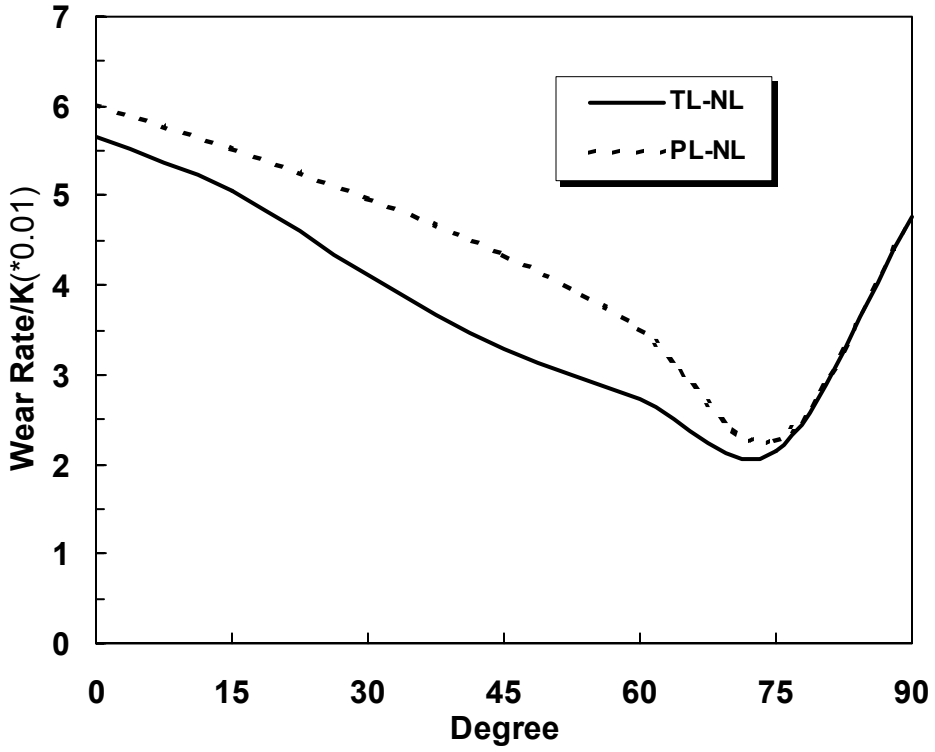

Figure 28 Theoretical wear trend for T300/Epoxy from PL/TL (0deg) to NL (90deg)

Another interesting trend in Fig. 28 is that the predicted wear rate in the PL orientation is slightly larger than in the TL, which is inconsistent with the experimental result [2] that found the wear in TL was 1.4 times that in PL. This indicates that a two-dimensional plane stress model is not sufficient to discern the wear difference between the PL and the TL orientations. A three-dimensional geometrical model is required to accommodate the difference of the shear stress strength among three principal material orientations for highly anisotropic materials

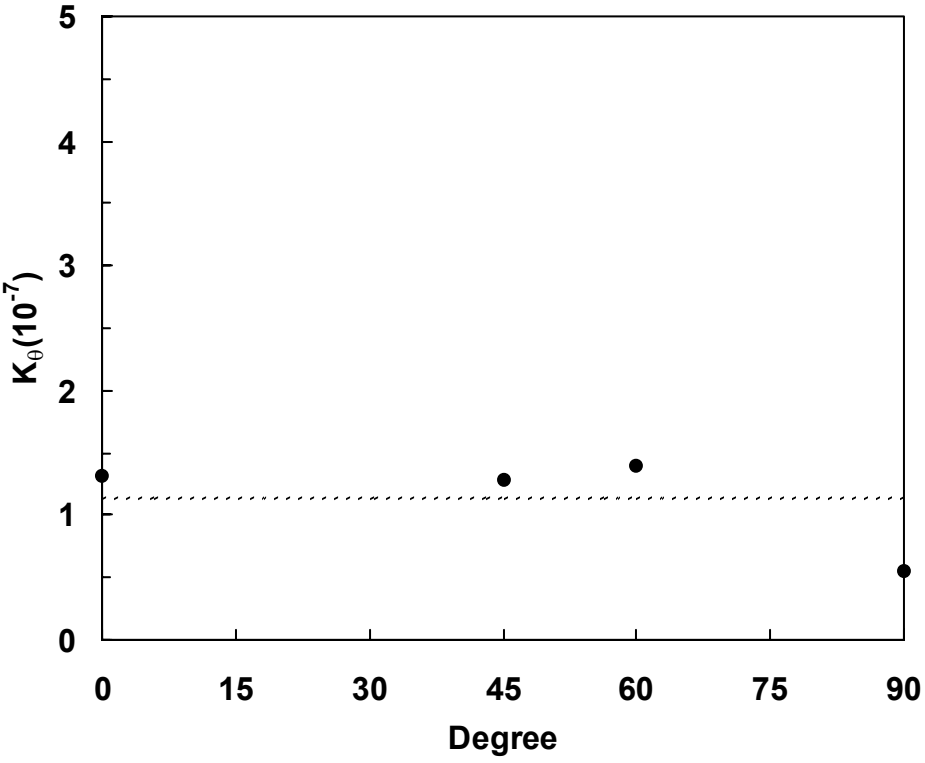

Figure 29 Verification of the results from TL (0deg) to NL (90deg)

Table 5 Material strength of T300/Epoxy FRP composites

FRP	Strength			
Epoxy + T300 (Carbon fiber) [2]	Longitudinal tensile strength (MPa)	Longitudinal compression strength (MPa)	Transverse tensile strength (MPa)	Shear strength (MPa)
	1380	-1000	69	110

Table 6 Verification of the predicted data for T300/Epoxy

Fiber orientation		TL	45°	60°	NL
Test data (10^{-9}cm^3 kg^{-1} m^{-1})[2]	$\dot{w}$	7.4	4.2	3.8	2.8
Theoretical (10^{-2})	P_{max}/σ_x	5.65	3.28	2.73	4.76
Wear factor (10^{-7} cm^3 kg^{-1} m^{-1})	k_θ	1.30	1.28	1.39	0.55

5.5 Conclusion

In this investigation, anisotropic strength theories are employed to analyze the wear of FRP composites. A tentative anisotropic wear model is constructed to predict the anisotropic wear of composites based on the anisotropic strength and the contact behavior. Compared with the experimental data, the predicted results for the wear rate from TL to NL demonstrate a reasonable accuracy. One benefit of this wear model is that it may be used to tailor or optimize the tribological performance of unidirectional continuous FRP composites.

6.0 AXISYMMETRIC CONTACT OF A THIN, TRANSVERSELY ISOTROPIC ELASTIC LAYER

In the previous sections, the 2-D contact behavior of FRP composites have been evaluated. When transversely isotropic materials are in the form of a thin coating, their contact performance is different from that of the half-plane. In industrial applications, transversely isotropic solid lubricants are generally coated on the surface of components to prevent wear. Thus, it is essential to investigate the contact characteristics of thin, transversely isotropic elastic coatings.

6.1 Problem Formulation

In this section, an infinite, transversely isotropic layer on a rigid foundation will be considered. The elastic layer has uniform thickness t and its axis of material symmetry is normal to the plane of contact between the layer and the foundation. The free surface of the elastic layer is indented by a smooth, rigid spherical indenter of radius R (Fig.30). The central indentation depth is w^*. The radius of the contact patch is a, and the load P applied to the indenter is in the direction normal to the free surface of the layer. Due to the symmetry of the problem, the displacement and stress fields caused by the indentation will be cylindrically symmetric about an axis normal to the free surface of the layer that passes through the centroid of the spherical indenter.

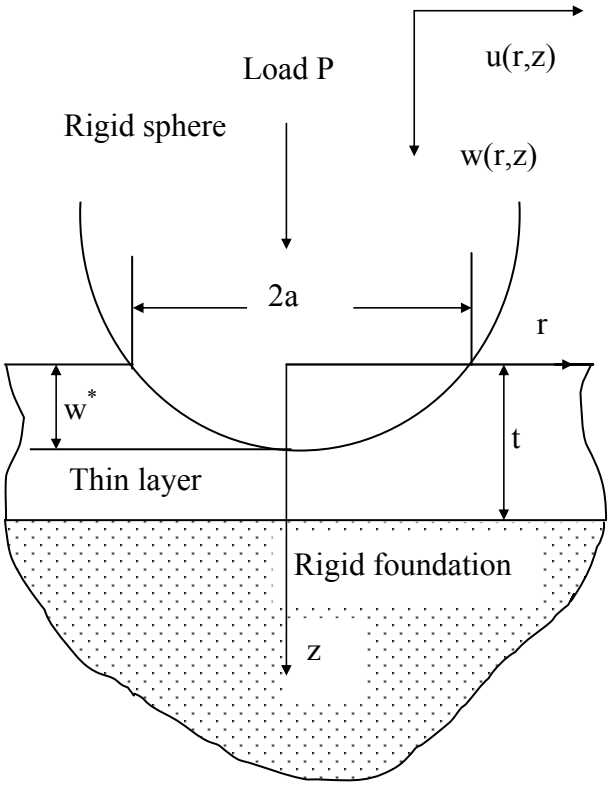

Figure 30 Geometry of the contacting surfaces

6.1.1 Governing Equations

Define a cylindrical coordinate system *(r, θ, z)* associated with an orthonormal vector basis $\{\hat{e}_r, \hat{e}_z, \hat{e}_\vartheta\}$, such that the *z*-axis is coincident with the problem's axis of symmetry and the elastic layer occupies the region $0 \le z \le t$, with *z*=0 at the layer's free surface and z=t at the layer/foundation interface (Fig.30). Given the cylindrical symmetry of the solution, the displacement field $\hat{u} = u_r\hat{e}_r + u_z\hat{e}_z + u_\theta\hat{e}_\theta$ has scalar components that can be represented by

$$u_r = u_r(r,z) \qquad u_z = u_z(r,z) \qquad u_\theta = 0 \tag{6.1}$$

It follows that the scalar components of the strain field are given by

$$\varepsilon_{rr} = \frac{\partial u_r}{\partial r},\ \varepsilon_{\theta\theta} = \frac{u_r}{r},\ \varepsilon_{zz} = \frac{\partial u_z}{\partial z},\ \varepsilon_{rz} = \frac{1}{2}\left(\frac{\partial u_r}{\partial z} + \frac{\partial u_z}{\partial r}\right), \varepsilon_{r\theta} = \varepsilon_{\theta z} = 0 \tag{6.2}$$

and that the transversely isotropic stress-strain constitutive relations reduce to

$$\begin{bmatrix} \sigma_{rr} \\ \sigma_{\theta\theta} \\ \sigma_{zz} \\ \sigma_{rz} \end{bmatrix} = \begin{bmatrix} c_{11} & c_{12} & c_{13} & 0 \\ c_{12} & c_{11} & c_{13} & 0 \\ c_{13} & c_{13} & c_{33} & 0 \\ 0 & 0 & 0 & c_{44} \end{bmatrix} \begin{bmatrix} \varepsilon_{rr} \\ \varepsilon_{\theta\theta} \\ \varepsilon_{zz} \\ 2\varepsilon_{rz} \end{bmatrix} \tag{6.3}$$

with $\sigma_{r\theta} = \sigma_{\theta z} = 0$

where σ_{ij} are the scalar components of the stress field in the layer and c_{ij} are the transversely isotropic elastic constants. Finally, the equilibrium equations reduce to

$$\frac{\partial \sigma_{rr}}{\partial \mathrm{r}} + \frac{\partial \sigma_{rz}}{\partial \mathrm{z}} + \frac{\sigma_{rr} - \sigma_{\theta\theta}}{\mathrm{r}} = 0 \tag{6.4}$$

$$\frac{\partial \sigma_{rz}}{\partial \mathrm{r}} + \frac{\partial \sigma_{zz}}{\partial \mathrm{z}} + \frac{\sigma_{\mathrm{rz}}}{\mathrm{r}} = 0 \tag{6.5}$$

where the third equilibrium equation is trivially satisfied.

6.1.2 Boundary Conditions

Two different interface conditions between the elastic layer and the rigid foundation will be considered. The elastic layer will either be assumed to be: (1) ideally bonded to the foundation; (2) lying frictionless (unbonded) on the interface.

At the free surface of the layer (z=0), tractions are zero in the contact patch,

$$\sigma_{\mathrm{rz}} = \sigma_{zz} = 0 \quad \text{when} \quad z = 0\,,\ 0 \le r \le a \tag{6.6}$$

while at the layer/indenter interface, the tangential traction is zero and the normal displacement is given by the spherical profile of the indenter,

$$\sigma_{\mathrm{rz}} = 0,\ \ u_{\mathrm{z}} = w(r) \quad \text{when} \quad z = 0\,,\ r \le a \tag{6.7}$$

where $w = w^* - R + \sqrt{R^2 - r^2} = w^* - R + R\sqrt{1-(r/R)^2}$. If r<<R, $\sqrt{1-(r/R)^2} \approx 1 - r^2/2R^2$, then

$$w(r) \approx w^* - \frac{r^2}{2R} \tag{6.8}$$

Note the requirement that $w(a) = 0$, it follows that for a thin elastic layer

$$w^* = \frac{a^2}{2R} \tag{6.9}$$

- *Ideally bonded interface*

  For the ideally bonded case, there is zero displacement at the layer/foundation interface,

$$u_r\big|_{z=t} = u_z\big|_{z=t} = 0 \quad \forall r \in [0, \infty) \tag{6.10}$$

- *Frictionless (unbonded) interface*

  For the frictionless case, the tangential traction and the normal displacement are zero at the layer/foundation interface,

$$\sigma_{rz} = 0, \quad u_z = 0 \ \text{ when } \ z = t \tag{6.11}$$

6.2 Approximate Solutions

The axisymmetric generalization of Johnson's assumption [29] that ' plane section remains plane after compression' implies that the radial displacement is independent of z. To begin, note that this assumption implies that

$$\sigma_{rz} = c_{44} \frac{\partial u_z}{\partial r} \tag{6.12}$$

which means that, at the interface between the indenter and the elastic layer, the zero-friction boundary condition Eq. 6.7_1 and the normal displacement boundary condition Eq. 6.7_2 cannot be simultaneously satisfied. Priority here is given to the normal displacement boundary condition. On the other hand, the zero-friction boundary condition Eq. 6.11_1 is implied by the zero normal displacement boundary condition Eq. 6.11_2.

Given the assumed form of the displacement field, it will not be possible to find solutions of the equilibrium equations Eq. 6.4 and Eq. 6.5 that satisfy all of the boundary and internal continuity conditions. Accordingly, the solutions derived below will be approximate-they may be unequilibrated and/or some of the boundary and internal continuity conditions may not be satisfied. Te conditions that are not satisfied will be explicitly identified and some indication of the degree of error will be given via comparison with finite element analysis.

6.2.1 Unbonded, Frictionless Interface

a. Approximate Method 1: negligible shear stress

One possible approximation is to assume that the shear stress in the contact zone and throughout the layer is identically zero,

$$\sigma_{rz} = 0 \tag{6.13}$$

and the compression strain is approximately averaged throughout the layer thickness,

$$\varepsilon_{zz} \cong \overline{\varepsilon_{zz}}(r) \qquad (t << a) \tag{6.14}$$

It follows from Eq. 6.2_3 and the axial displacement boundary conditions Eq. 6.7_2 and 6.11_2 that

$$u_z = (1 - \frac{z}{t}) w(r) \tag{6.15}$$

Hence, substituting Eq. 6.13 and Eq. 6.15 with Eq. 6.2 and Eq. 6.3 into Eq. 6.4 yields:

$$r^2 \frac{\partial^2 u_r}{\partial r^2} + r \frac{\partial u_r}{\partial r} - u_r = -\frac{c_{13} r^3}{c_{11} R t} \tag{6.16}$$

The general and particular solution to this Euler-Cauchy equation is

$$u_r = B_1 r + B_2 \frac{1}{r} - \frac{c_{13} r^3}{8 c_{11} R t} \tag{6.17}$$

The requirement that the displacement at r=0 is finite makes B_1 =0. Substituting Eq. 6.15 and Eq. 6.17 into Eqs. 6.2 and 6.3 requiring that $\sigma_{zz}\big|_{z=0} = 0$ vanish as $r \to a$ then gives

$$\sigma_{zz} = \frac{c_{13}^2 - c_{11} c_{33}}{2 c_{11} R t} (a^2 - r^2) \tag{6.18}$$

Thus the contact pressure is

$$p(r) = -\sigma_{zz} = \frac{c_{11} c_{33} - c_{13}^2}{2 c_{11} R t} (a^2 - r^2) \tag{6.19}$$

The total applied load can then be integrated over the contact patch:

$$P = \int_0^a 2\pi r p(r) dr \tag{6.20}$$

After integrating the above equation and transforming, the contact radius is

$$a = \left(\frac{4Pc_{11}Rt}{\pi(c_{11}c_{33} - c_{13}^2)}\right)^{\frac{1}{4}} \tag{6.21}$$

Note that, in this case, the contact pressure distribution and contact patch radius are independent of the elastic constant c_{44}.

b. Approximate method 2: considering shear stress

Given this assumed form of the displacement field, it follows from Eqs. 6.2-6.5 that the equilibrium equations reduce to

$$r^2 f''(r) + rf'(r) - f(r) = -\frac{c_{13} + c_{44}}{c_{11}} r^2 \frac{\partial^2 u_z}{\partial r \partial z} \tag{6.22}$$

$$c_{44}\frac{\partial^2 u_z}{\partial r^2} + c_{33}\frac{\partial^2 u_z}{\partial z^2} + \frac{c_{44}}{r}\frac{\partial u_z}{\partial r} = 0 \tag{6.23}$$

It follows from Eq. 6.22 that $\partial^2 u_z / \partial r \partial z$ is independent of z. Using this as a starting point, one can obtain a general solution for u_z from Eq. 6.23,

$$u_z = A_1 z r^2 - \frac{2c_{44}}{3c_{33}} A_1 z^3 + A_2 z \ln r - A_3 r^2 + \frac{2c_{44}}{3c_{33}} A_3 z + A_4 \ln r + A_5 z + A_6 \tag{6.24}$$

and then a general solution u_r from Eq. 6.22

$$u_r = A_7 + \frac{A_8}{r} - \frac{c_{13} + c_{44}}{4c_{11}}(A_1 r^3 + 2A_2 r \ln r) \tag{6.25}$$

where A_n, n = 1…8 , are constants. Thus, Eqs. 6.24 and 6.25 represent the most general form of equilibrated, axisymmetric displacement field consistent with the assumption that plane sections remain plane.

The zero normal displacement condition, $u_z\big|_{z=t} = 0$ for all $r \in [0,\infty)$, at the interface between the elastic layer and the rigid foundation, the normal displacement condition, $u_z\big|_{z=0} = (a^2 - r^2)/2R$ for all $r \in [0,a]$, at the interface between the elastic layer and the spherical indenter, the requirement that u_r vanish at r=0, and the requirement that $\sigma_{zz}\big|_{z=0} = 0$ vanish as $r \to a$ a reduce the equilibrated displacement field Eqs. 6.24-6.25 to

$$\left.\begin{aligned} u_z &= (1-\frac{z}{t})\frac{a^2-r^2}{2R} + \frac{c_{44}}{3c_{33}R}(t-z)(2t-z) \\ u_r &= \frac{c_{44}tr}{3c_{13}R} + \frac{c_{13}+c_{44}}{8c_{11}Rt}(2a^2r - r^3) \end{aligned}\right\} \quad \forall r \in [0,a] \tag{6.26}$$

The approximate solution does not satisfy the zero-friction boundary condition Eq. 6.7_1. Additionally, the approximate solution for $0 \le r \le a$ is independent of the response of the elastic layer outside of this domain.

Substituting Eq. 6.26 into Eqs. 6.1-6.3 and using the boundary conditions at $r = \pm a$, the contact pressure is given by:

$$p(r) = -\sigma_{zz} = \frac{c_{11}c_{33} - c_{13}(c_{13}+c_{44})}{2c_{11}Rt}(a^2 - r^2) \tag{6.27}$$

and the contact radius is

$$a = \left(\frac{4Pc_{11}Rt}{\pi[c_{11}c_{33} - c_{13}(c_{13} + c_{44})]}\right)^{\frac{1}{4}} \tag{6.28}$$

6.2.2 Ideally Bonded Interface

If the layer is ideally bonded on the rigid foundation, the radial displacement on the surface of z=t is fixed. When Johnson's assumption is applied, it means that the radial displacement of the thin layer is identically zero throughout the layer thickness, i.e.

$$u_r(r,z) = 0, \qquad \varepsilon_{rr}(r,z) = 0 \tag{6.29}$$

Physically Eq. 6.29 implies that the plane sections of a thin layer remain motionless.

It is important to note that the axial displacement boundary conditions Eq. 6.7_2 and Eq. 6.10_2 and the equilibrium equations Eqs. 6.4 and 6.5 are incompatible with this result, that is, they cannot be simultaneously satisfied. Thus, the decision is made to satisfy the axial displacement boundary conditions at the expense of the equilibrium equations.

Assume that the strain component ε_{zz} is uniform though the thickness of the elastic layer:

$$\varepsilon_{zz} \cong \overline{\varepsilon_{zz}}(r) \tag{6.30}$$

It follows from the strain-displacement relations Eq. 6.2_3, the axial displacement boundary conditions Eq. 6.6_2 and Eq. 6.10_2, and the traction-free boundary condition outside the contact patch that

$$u_z = \begin{cases} \dfrac{a^2 - r^2}{2Rt}(t - z), & \forall r \in [0, a] \\ 0, & \forall r \in [a, \infty) \end{cases} \tag{6.31}$$

Substituting Eq. 6.31 into Eq. 6.3$_3$ yields:

$$\sigma_{zz} = c_{33}\varepsilon_{zz} = -c_{33}\frac{(a^2 - r^2)}{2Rt} \tag{6.32}$$

The contact pressure between the indenter and the elastic layer is

$$p(r) = -\sigma_{zz} = \frac{c_{33}}{2Rt}(a^2 - r^2) \tag{6.33}$$

The total applied load is

$$\begin{aligned} P &= \int_{-a}^{+a} 2\pi r p(r) dr = 2\pi \int_{0}^{+a} \frac{c_{33} r(a^2 - r^2)}{2Rt} dr \\ &= \frac{\pi a^4 c_{33}}{4Rt} \end{aligned} \tag{6.34}$$

and the contact radius for a bonded thin layer is

$$a = \left(\frac{4RtP}{\pi c_{33}} \right)^{\frac{1}{4}} \tag{6.35}$$

It is interesting to note that the contact pressure Eq. 6.33, and the profile for transversely isotropic thin coatings bonded to the foundation are independent of four of the five elastic constants.

6.3 Results And Discussion

6.3.1 Reduced Solutions For Isotropic Materials

In order to initially evaluate the accuracy of the analytical expressions introduced in this work, we will examine the reduced solutions for the case of isotropic coatings. The relationships between elastic constants for transversely isotropic materials are as follows:

$$c_{11} = c_{22} = \frac{1 - \nu_{23}\nu_{32}}{E_2 E_3 \Delta} \tag{6.36}$$

$$c_{13} = c_{23} = \frac{\nu_{31} + \nu_{21}\nu_{32}}{E_2 E_3 \Delta} = \frac{\nu_{13} + \nu_{12}\nu_{23}}{E_1 E_3 \Delta} \tag{6.37}$$

$$c_{33} = \frac{1 - \nu_{12}\nu_{21}}{E_1 E_3 \Delta} \tag{6.38}$$

where $\Delta = \frac{1 - \nu_{12}\nu_{21} - \nu_{23}\nu_{32} - \nu_{13}\nu_{31} - 2\nu_{21}\nu_{32}\nu_{13}}{E_1 E_2 E_3}$. For isotropic elastic materials with $\nu_{ij}=\nu\neq 0.5$ and $E_i=E$, the solutions Eqs. 6.19-6.21 and Eqs. 6.33-6.35 are immediately reduced to the Jaffar's formulae [31] for isotropic elastic materials. For example, the pressure distributions Eq. 6.19 and Eq. 6.33 for the transversely isotropic materials may be simplified to Jaffar's solutions Eqs. 6.39 and 6.40, respectively.

For frictionless layer:

$$p(r) = \frac{E}{1-\nu^2}\frac{(a^2 - r^2)}{2Rt} \tag{6.39}$$

For bonded layer:

$$p(r) = \frac{(1-\nu)^2}{1-2\nu}\frac{E}{1-\nu^2}\frac{(a^2 - r^2)}{2Rt} \tag{6.40}$$

Jaffar's solutions are for isotropic elastic materials. Therefore, the present solutions Eqs. 6.19-6.21 and Eqs. 6.33-6.35 may be taken as the extension of Jaffar's solutions to a transversely isotropic elastic material. However, the solution Eq. 6.27 cannot be reduced to the solution Eq. 6.39 for isotropic materials. This is due to the fact that the approximate method employed in deriving Eq. 6.27 is different from that of Jaffar's. As will be discussed in the following section, the solutions Eq. 6.19 and Eq. 6.33 provide more accurate approximate results than the solution Eq. 6.27.

6.4 Comparison With Finite Element Analysis

6.4.1 FEM Model

In order to further ascertain the accuracy of the solutions presented in this work, the results of the asymptotic transversely isotropic analyses were compared to those generated with the finite element method (FEM). The commercial FEM software ABAQUS 6.1 was adopted to simulate the stress and displacement of a transversely isotropic elastic thin layer that was either bonded or lying frictionless on a rigid foundation.

The finite element model consisted of a rigid spherical indenter that was in normal contact with a coating layer. The element type for the coating layer was a 2-D axi-symmetric element, while the element type for the indenter was an analytical rigid surface with a 8mm radius. The dimensions of the layer were 1mm long and 5μm thick. With a mesh size of 5μm×0.5μm, there were approximately 2000 elements within the layer. At the bottom edge of the layer, both the horizontal and vertical displacements were constrained for a bonded condition. Only vertical displacement constraints were applied for an unbonded layer. Axi-symmetry was defined so that horizontal displacements were constrained along the left-hand side of the layer. According to the designated ratio of the contact radius to layer thickness, a known vertical displacement was applied to the indenter.

The elastic constants of the transversely isotropic material $NbSe_2$ are c_{11}=105 GPa, c_{33}=54 GPa, c_{12}=14 GPa, c_{13}=31 GPa, and c_{44}=19.5 GPa. Considering the directions of the

geometry examined, c_{33} was the elastic constant in the principal direction of the transversely isotropic plane of the layer, which was perpendicular to the contact plane. c_{11} and c_{22} were the elastic constants parallel to the contact plane.

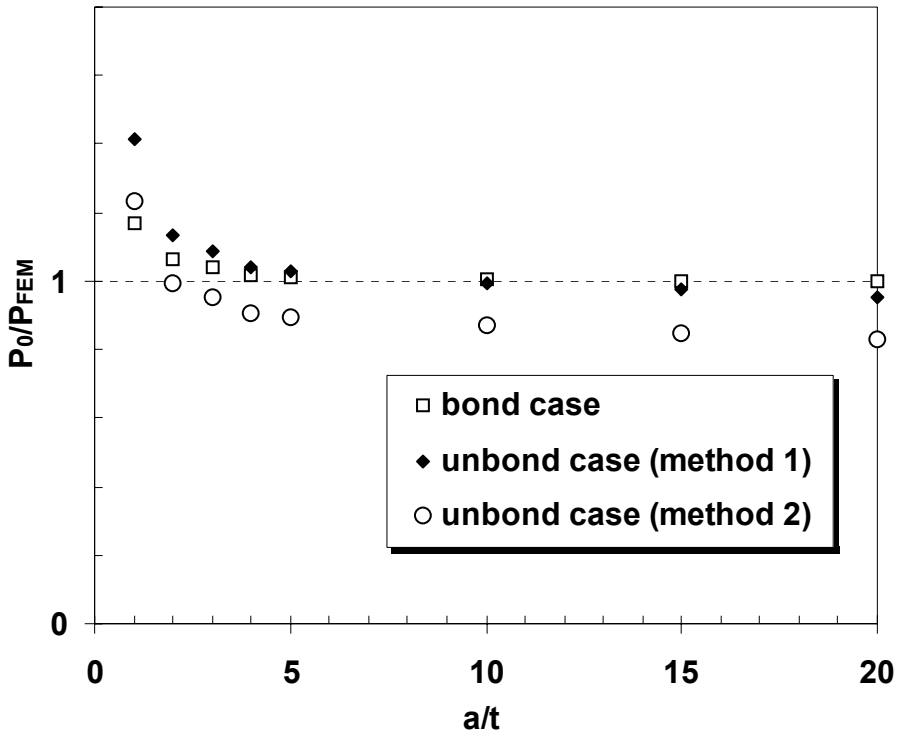

Figure 31Comparison between the predicated maximum contact pressure p(0) and the FEM results

6.4.2 Comparison For Bonded Layer

The numerical results are compared to the approximate bonded layer solution Eq.6.33 in Figs. 31 and 32. Examining Fig. 31, it is found that the results predicted by equation Eq. 6.33 for the bonded layer are in very good agreement with those determined by FEM. This is particularly true when the ratio of the contact radius to layer thickness is larger than 2.0. As shown in Fig. 31, the predicted results are slightly larger than those by FEM, but converge very close to the FEM results when a/t >10. The pressure distribution on the contact interface is parabolic in nature, as shown in Fig. 32.

6.4.3 Comparison For Unbonded Layer

The results of FEM and the approximate solutions (Eqs. 6.19 and 6.27) for the unbonded layer are compared and plotted in Figs. 31 and 32. From Fig. 31, it is found that the result using the method of negligible shear stress in an unbonded layer diverges from FEM when a/t becomes larger than 10. When 5< a/t <10, however, the predicted results of Eq. 6.19 converges to the FEM values. Examining the overall results of Eqs. 6.19 and 6.27, it is found that by considering the shear stress yields substantially poorer results than Eq. 6.19. It shows that the results of Eq. 6.27 are significantly smaller than FEM results. From Fig. 32, it is found that the contact pressure distribution on the surface of a thin unbonded layer is also parabolic, as predicted by the solutions of Eqs. 6.19 and 6.27.

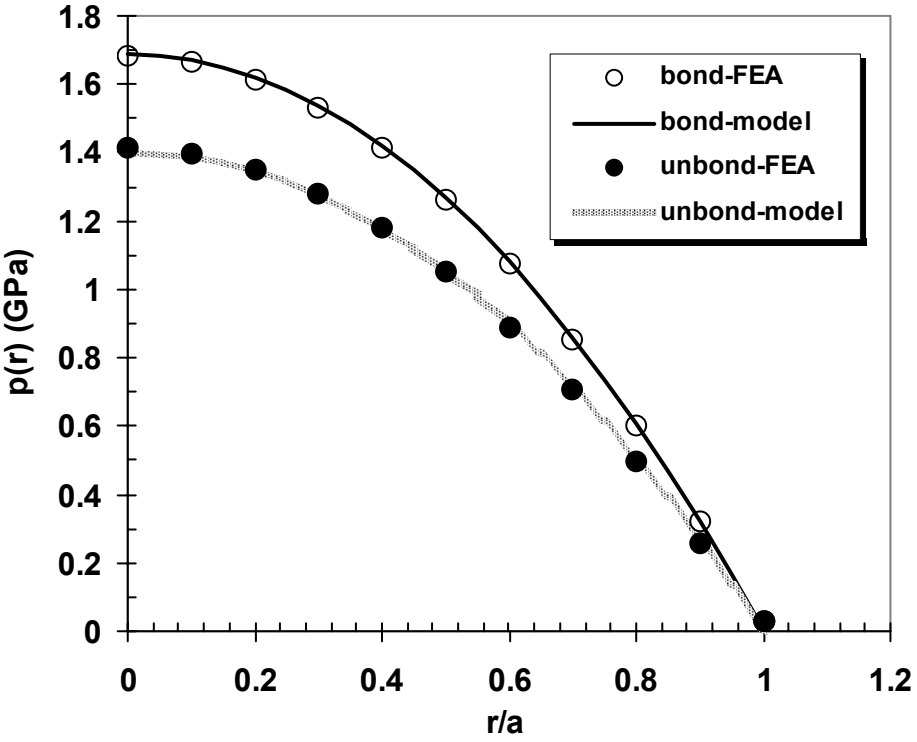

Figure 32 Contact pressure for the bonded and unbonded cases

6.5 Conclusion

The contact problem of a rigid sphere on a thin transversely isotropic elastic layer was analyzed in this section. Both the conditions of a layer being ideally bonded and lying frictionless (unbonded) on a rigid foundation have been considered. For the bonded layer, a solution was obtained using Johnson's assumption [29]. In the case of the unbonded layer, two approximate solutions were also similarly obtained using Johnson's assumption by assuming negligible and non-negligible shear stress. Results for each solution were then compared to FEM predicted values to ascertain their relative accuracy. From the analytical solutions, and their comparison to FEM values, the following conclusions were drawn:

- The approximate solutions for the bonded layer or the unbonded layer with negligible shear stress were found to reduce to Jaffar's solution for an isotropic layer. In contrast, the unbonded layer solutions considering shear stress did not reduce to the isotropic solution.
- With an increase of the ratio of the contact radius to layer thickness (a/t), the bonded layer results converge to the FEM values whereas the unbonded results with negligible shear stress in the layer become less accurate.
- The pressure distributions for all of the conditions were found to be parabolic in nature.
- For the unbonded layer, the results obtained for neglecting the shear stress were found to be more accurate than those obtained by considering the shear stress.

7.0 SUMMARY AND FURTHER CONSIDERATION

In this work, three objectives were achieved. First, the anisotropic contact behaviors of FRP composites were evaluated by incorporating a closed-form sliding contact solution, analytical or explicit expressions of Barnett-Lothe tensors, and the elastic properties of FRP composites. The effects of matrix material, friction coefficient, fiber material, fiber orientation and fiber volume fraction on the contact characteristics of FRP composites were investigated. From the analytical data, several important tendencies for FRP composites have been determined, as related to optimizing the tribological performance of FRP materials. These findings are:

1) The maximum contact pressure and contact width of FRP composites are dominated by the elastic stiffness in the normal contact direction, and therefore the largest maximum contact pressure and the smallest contact area occur as the sliding direction is obtained in the NL orientation. And the lowest maximum contact pressure was obtained in the transverse fiber orientation.
2) The maximum contact pressure and the contact width were found to monotonically vary as the fiber orientation was rotated between PL, NL, and TL orientations.
3) Based on the comparison with the experiment data, the level of contact deformation in FRP composites was found to correlate with the wear rate. Therefore, similar to that found by experiments [2, 7], the NL fiber orientation possesses the highest wear resistance.
4) The frictional sliding pressure distributions of FRP materials were not symmetrical, as the maximum contact pressure is inclined to the sliding direction. The contact symmetry parameter δ was found to be highly dependent on the fiber orientation. The contact

pressure distribution in the normal fiber alignment has the least symmetric contact area, whereas the parallel fiber alignment is the most symmetric.

5) With a variation of fiber materials, the contact pressure in the transverse and parallel fiber orientations show little change. In the normal fiber alignment, however, fiber materials significantly influence the contact behavior. This trend was attributed to the fact that the fibers carry a substantial portion of the normal load in the NL direction, and therefore is more sensitive to fiber material properties.
6) Since fibers are several hundred times stiffer than matrix materials, increasing the fiber volume fraction of FRP composites increases the maximum contact pressure in all the three fiber alignments.
7) The elastic modulus of the matrix material also has a strong influence on the maximum contact pressure distribution. The normal orientation was least sensitive to changes in matrix materials.
8) The frictional coefficient of FRP composites has little influence on the magnitude of the contact pressure in all the three fiber orientations. The magnitude of the friction coefficient did have a significant influence on the symmetry of the contact patch, except for the PL orientation.

Furthermore, the anisotropic failure strength theory was utilized to account for the significant anisotropy of the wear in FRP composites. Based on the anisotropic failure strength criteria an anisotropic wear model was proposed. The theoretically predicated wear results were in good agreement with the published experimental data. It demonstrates the failure strength theory is highly related to the anisotropy of wear in FRP composites.

Finally, starting from the theory of elasticity and the basic assumptions, a set of approximate equations were obtained for a thin, transversely isotropic coating on rigid foundations.

Based on the present work, the further research should be done in the two areas. The first work is to extend the present analysis approach to investigate the contact behavior of the metal / ceramics matrix composites. The second is to determine the applicability and validation of the proposed anisotropic strength method and the wear model for FRP composite by performing extensive experiments for various FRP composite materials.

BIBLIOGRAPHY

BIBLIOGRAPHY

[1] Jost, P., 1966, *Lubrication (tribology)-a report on the present position and industry's needs*, Department of Education and Science, H. M. Stationary Office, London

[2] Sung, N.-H., Suh, N. P., 1978, "Effect of fiber orientation on friction and wear of fiber reinforced polymeric composites," Wear, **53**, pp.129-141

[3] Lhymn, C., 1987, "tribological properties of unidirectional polyphenylene sulfide-carbon laminate composites", Wear, **117**, pp147-159

[4] Cirino, M., Friedrich, K., Pipes, R. B., 1988, "The effect of fiber orientation on the abrasive wear behavior of polymer composite materials," Wear, **121**, pp.127-141

[5] Vishwananth, B., Verma, A. P., Rao, V. S. K., 1993, "Effect of reinforcement on friction and wear of fabric reinforced polymer composites," Wear, **167**, pp.93-99

[6] Shim, H. H., Kwon, O. K., Youn, J. R., 1992, "Effects of fiber orientation and humidity on friction and wear properties of graphite fiber composites", Wear, **157**, pp141-149

[7] Tsukizoe, T., Ohmae, N., 1986, "Friction and wear performance of uni-directionally oriented glass, carbon, aramid and stainless steel fibre reinforced plastics, friction and wear of polymer composites," *Friction and Wear of Polymer Composites*, Friedrich, K, ed., Elsevier, NY, pp. 205-231

[8] Ovaert, T. C., Wu, J. -P., 1993, "Theoretical estimates of asperity-scale stresses in normally-oriented continuous fiber-reinforced composites," STLE Tribology Transactions, **36**, pp.120-126

[9] Wu, J. -P., Ovaert, T. C., 1994, "Effect of asperity-scale tensile stresses on the wear behavior of normally oriented fiber reinforced composites," STLE Tribology Transactions, **37**, pp.23-32

[10] Ovaert, T. C., 1995, "On the wear behavior of longitudinally (parallel) oriented unidirctional fiber-reinforced polymer composites," STLE Tribology Transactions, **38**, pp.27-34

[11] Ovaert, T.C., 1997, "Wear of unidirectional polymer matrix composites with fiber orientation in the plane of contact," STLE Tribology Transactions, **40**, pp.227-234

[12] Klintworth, J. W., Stronge, W. J., 1990, "Plane punch indentation of anisotropic elastic half space", ASME J. of Applied Mechanics, **57**, pp.84-90

[13] Fan, H., Keer, L. M., 1994, "Two-dimensional contact on an anisotropic elastic half-space", ASME J. of Tribology, **250**, pp. 250-255

[14] Muskhelishvili, N. L, *Some Basic Problems of the Mathematical Theory of Elasticity*, Noodhoff, Gronigen, 1953

[15] Stroh, A. N., 1958, "Dislocation and cracks in anisotropic elasticity," Philosophical Magazine, **3**, pp.625-646

[16] Fan, C. W., Hwu, C., 1996, "Punch problems for an anisotropic elastic half-plane," ASME Journal of Applied Mechanics, **63**, pp.69-76

[17] Hwu, C., Fan, C.W., 1998, "Sliding punches with or without friction along the surface of an anisotropic elastic half-plane," Quarter Journal of Mechanics and Applied Mathematics, **51**, pp.159-177

[18] Hwu, C., Fan, C.W., 1998, "Contact problem of two dissimilar anisotropic elastic bodies," ASME Journal of Applied Mechanics, **65**, pp.580-587

[19] Ning, X., Lovell, M. R., 2002, "On the Sliding Friction Characteristics of Unidirectional Continuous FRP Composites", ASME Trans. J. of Tribology, **124**, pp.5-13

[20] Ning, X., Lovell, M. R., Slaughter, W., 2002, "Two-dimensional anisotropic contact behavior of unidirectional continuous FRP composites", (to appear in J. of Tribology)

[21] Lovell, M. R., and Khonsari, M. M., and Marangoni, R. D., 1997, "Parameter identification of hysteresis friction for coated ball bearings based on three dimensional FEM analysis," ASME Journal of Tribology, **119**, pp. 462-470

[22] Sneddon, I. N., 1964, *Fourier Transforms*, New York, Toronto, and London: McGraw-Hill

[23] Chen, W. T., 1971, "Computation of stresses and displacements in a layered elastic medium," International Journal of Engineering Science, **9**, pp. 775-800

[24] Chen, W. T., and Engel, P. A., 1972, "Impact and contact stress analysis in multiplayer media," International Journal of Solids and Structures, **8**, pp. 1257-1281

[25] Matthewson, M. J., 1981, "Axi-symmetric contact on thin compliant coatings," Journal of Mechanics and Physics of Solids, **29**, pp. 89-113

[26] Aleksandrov,V. M., 1967, "On the approximate solution of some integral equations of the theory of elasticity and mathematical physics, " Journal of Applied Mathematics and Mechanics, **31**, pp.1117-1131

[27] Jaffar, M. J., 1988, "A numerical solution for axismmetric contact problems involving rigid indenters on elastic layers," Journal of Mechanics and Physics of Solids, **36**, pp. 401-416

[28] O'Sullivan, T. C., and King, R. B., 1988, "Sliding contact stress field due to a spherical indenter on a layered elastic half-space," ASME Journal of Tribology, **110**, pp. 235-240

[29] Johnson, K. L., 1985, *Contact Mechanics*, Cambridge University Press, Cambridge, pp.138-141

[30] Meijers, P., 1968, "The contact problem of a rigid cylinder on an elastic layer," Applied Science Reserach, **18**. p. 353

[31] Jaffar, M. J., 1989, "Asymptotic behavior of thin elastic layers bonded and unbonded to a rigid foundation," International Journal of Mechanical Science, **31**, pp. 229-235

[32] Barber, J. R., 1990, "Contact problems for thin elastic layer," International Journal of Mechanical Science, **32**, pp. 129-132

[33] Tian, X., Bhushan, B., 1996, "A numerical three–dimensional model for the contact of rough surfaces by variational principle", ASME J. of Tribology, 118, pp.33-41

[34] Ovaert, T. C., 1993, "On the indentation of a transversely isotropic half-space with application to thin solid lubricant films," ASME Journal of Tribology, **115**, pp. 650-657

[35] Kuo, C. H., and Keer, L. M., 1992, "Contact stress analysis of layered transversely isotropic half-space," ASME Journal of Tribology, **114**, pp. 253-262

[36] Lovell, M. R., Khonsari, M. M., and Marangoni, R. D., 1997, "Frictional analysis of MoS_2 coated ball bearings: a three-dimensional finite element analysis," ASME Journal of Tribology, **119**, pp. 754-763

[37] Lovell, M. R., and Khonsari, M. M., 1999, "On the frictional characteristics of ball bearings coated with solid lubricants," ASME Journal of Tribology, **121**, pp. 761-767

[38] Dongye, C., Ting, T. C. T., 1989, "Explicit expressions of Barnett-Lothe tensors and their associated tensors for orthotropic materials," Quarterly Journal of Applied Mathematics, **47**, pp.724-734

[39] Yin, W.-L., 2000, "Deconstructing plane anisotropic elasticity Part II: Stroh's formalism sans frills" , International Journal of Solids and Structures, **37**, pp.5277-5296

[40] Rosen, B. W., 1973, "Stiffness of fiber composite materials," Composites, **4**, pp.16-25

[41] Hashin, Z., 1983, "Analysis of composite materials-a survey," ASME Journal of Applied Mechanics, **50**, pp.481-505

[42] Ting, T.C.T., 1998, "symmetric representation of stress and strain in the Stroh formalism and physical meaning of the tensors L, S, L(θ) and S(θ)", **50**, pp. 91-96

[43] Suh, N. P., 1986, *Tribophysics*, Prentice-Hall, Inc.

[44] Bhushan, B., 1999, *Principles and Applications of Tribology*, John Wily & Sons, Inc., p485, p500

[45] Jones, R. M., 1999, *Mechanics of Composite Materials*, Taylor & Francis, Inc., p101

[46] Herakovich, C. T., 1998, *Mechanics of Fibrous Composites*, John Wily & Sons, Inc., p316

[47] Tsai, S. W., Wu, E. M., 1971, "A general theory of strength for anisotropic materials", J. of Composite Materials, pp.58-80

[48] Narayanaswami, N., Adelman, H. M., 1977, "Evaluation of the tensor polynomial and Hoffman strength theories for composite materials", J. of Composite Materials, pp.366-377